Cell Metabolism

Article

Unveiling adipose populations linked to metabolic health in obesity

Graphical abstract

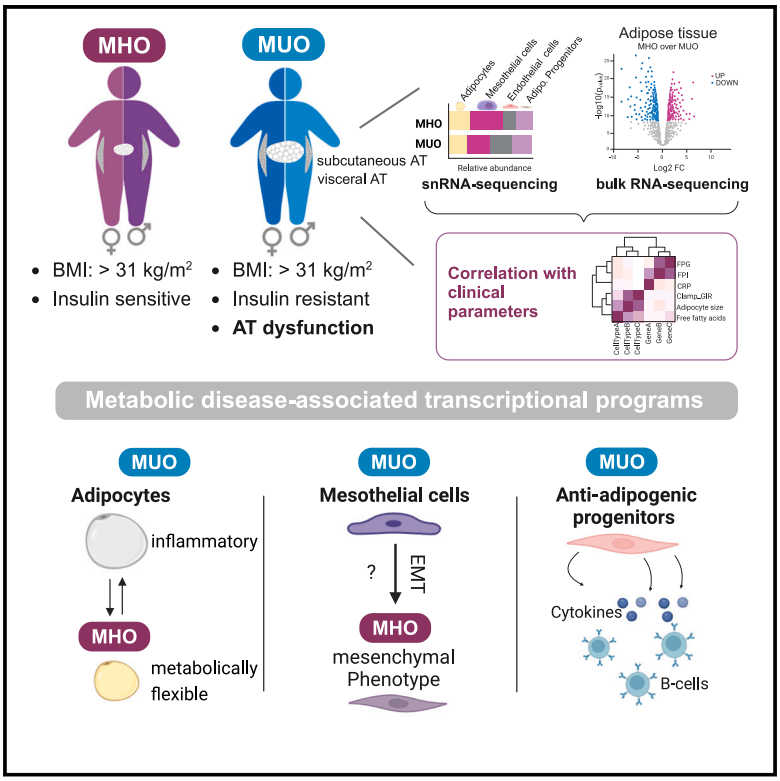

Highlights

- Single-nuclei adipose tissue atlas of metabolically healthy and unhealthy obesity
- Visceral adipose tissue is significantly remodeled in response to metabolic disease
- Adipocyte plasticity is strongly associated with metabolic health
- Mesothelial cells are linked to visceral adipose tissue dysfunction and metabolic disease

Authors

Isabel Reinisch, Adhideb Ghosh, Falko Noé, ..., Anne Hoffmann, Matthias Blüher, Christian Wolfrum

Correspondence

matthias.blueher@medizin.uni-leipzig.de (M.B.), christian-wolfrum@ethz.ch (C.W.)

In brief

Metabolic disease risk in individuals with obesity is variable and influenced by so-far-unknown factors. Reinisch and Ghosh et al. uncovered distinct cell populations and transcriptional programs in adipose tissue that are strongly linked to metabolic disease. The findings suggest that visceral adipose tissue plasticity is key to maintaining metabolic health despite excess adiposity.

Reinisch et al., 2025, Cell Metabolism *37*, 1–16
February 4, 2025
https://doi.org/10.1016/j.cmet.2024.11.006

CellPress

Cell Metabolism

CellPress
OPEN ACCESS

Article

Unveiling adipose populations linked to metabolic health in obesity

Isabel Reinisch,[1,8] Adhideb Ghosh,[1,2,8] Falko Noé,[1,2] Wenfei Sun,[1,3] Hua Dong,[1,4] Peter Leary,[2] Arne Dietrich,[5] Anne Hoffmann,[6] Matthias Blüher,[6,7,*] and Christian Wolfrum[1,9,*]

[1]Institute of Food, Nutrition and Health, ETH Zurich, Schwerzenbach, Switzerland
[2]Functional Genomics Center Zurich, ETH Zurich and University of Zurich, Zurich, Switzerland
[3]Department of Bioengineering, Stanford University, Stanford, CA, USA
[4]Stem Cell Bio Regenerative Med Institute, Stanford University, Stanford, CA, USA
[5]Department of Visceral, Transplant, Thoracic and Vascular Surgery, University Hospital of Leipzig, Leipzig, Germany
[6]Helmholtz Institute for Metabolic, Obesity and Vascular Research (HI-MAG) of the Helmholtz Zentrum München at the University of Leipzig and University Hospital Leipzig, Leipzig, Germany
[7]Medical Department III-Endocrinology, Nephrology, Rheumatology, University of Leipzig Medical Center, Leipzig, Germany
[8]These authors contributed equally
[9]Lead contact
*Correspondence: matthias.blueher@medizin.uni-leipzig.de (M.B.), christian-wolfrum@ethz.ch (C.W.)
https://doi.org/10.1016/j.cmet.2024.11.006

SUMMARY

Precision medicine is still not considered as a standard of care in obesity treatment, despite a large heterogeneity in the metabolic phenotype of individuals with obesity. One of the strongest factors influencing the variability in metabolic disease risk is adipose tissue (AT) dysfunction; however, there is little understanding of the link between distinct cell populations, cell-type-specific transcriptional programs, and disease severity. Here, we generated a comprehensive cellular map of subcutaneous and visceral AT of individuals with metabolically healthy and unhealthy obesity. By combining single-nucleus RNA-sequencing data with bulk transcriptomics and clinical parameters, we identified that mesothelial cells, adipocytes, and adipocyte-progenitor cells exhibit the strongest correlation with metabolic disease. Furthermore, we uncovered cell-specific transcriptional programs, such as the transitioning of mesothelial cells to a mesenchymal phenotype, that are involved in uncoupling obesity from metabolic disease. Together, these findings provide valuable insights by revealing biological drivers of clinical endpoints.

INTRODUCTION

The global obesity pandemic is worsening in many parts of the world resulting in an increased prevalence of associated sequelae.[1] Despite its strong association with the risk of morbidity, marked interindividual differences in the manifestation of cardiometabolic disease exist, with a subset of individuals with obesity being classified as metabolically healthy (metabolically healthy obesity [MHO]).[2] Considering the absence of type 2 diabetes, hypertension, dyslipidemia, and cardiovascular disease in these individuals, it is important to understand which cellular and molecular mechanisms define the metabolic heterogeneity in obesity.

Intra-abdominal adiposity is regarded as one of the strongest predictors of metabolic health risk, which can be attributed to the degree of adipose tissue (AT) dysfunction.[3–7] An expansion of adipocyte size can induce adipocyte stress-response transcriptional programs and AT remodeling, being characterized on the tissue level by changes in the cellular composition and tissue architecture.[8–10] Adding to the plasticity and heterogeneity of AT, impairments in the metabolic flexibility of adipocytes strongly alter the secretory profile of AT which can induce dysregulations in systemic energy homeostasis and enhance metabolic disease development.[8] Furthermore, the cellular landscape of AT is not only highly sensitive to different metabolic and pathological states but is also determined by the fat depot, gender, and age.[9] Considering the myriad functions of AT, any of these factors can affect the individual's risk to develop disease and may shape the heterogeneity among individuals with obesity.

Recent advances in single-cell and single-nucleus transcriptomics technologies provided new insights into the multiple layers of human AT heterogeneity, extending beyond the standard classification of AT-resident cell types.[11–14] These studies defined various cellular subpopulations in AT[10,11,14] and enabled a deep characterization of the cellular landscape of human AT in response to obesity progression.[11–13] However, the precise cell-specific mechanisms in AT that can uncouple obesity from metabolic disease development have not been elucidated yet.

In this project, we generated the first transcriptional atlas of human subcutaneous and visceral AT comparing people with MHO and metabolically unhealthy obesity (MUO). Our experimental design accounts for different aspects that

Please cite this article in press as: Reinisch et al., Unveiling adipose populations linked to metabolic health in obesity, Cell Metabolism (2024), https://doi.org/10.1016/j.cmet.2024.11.006

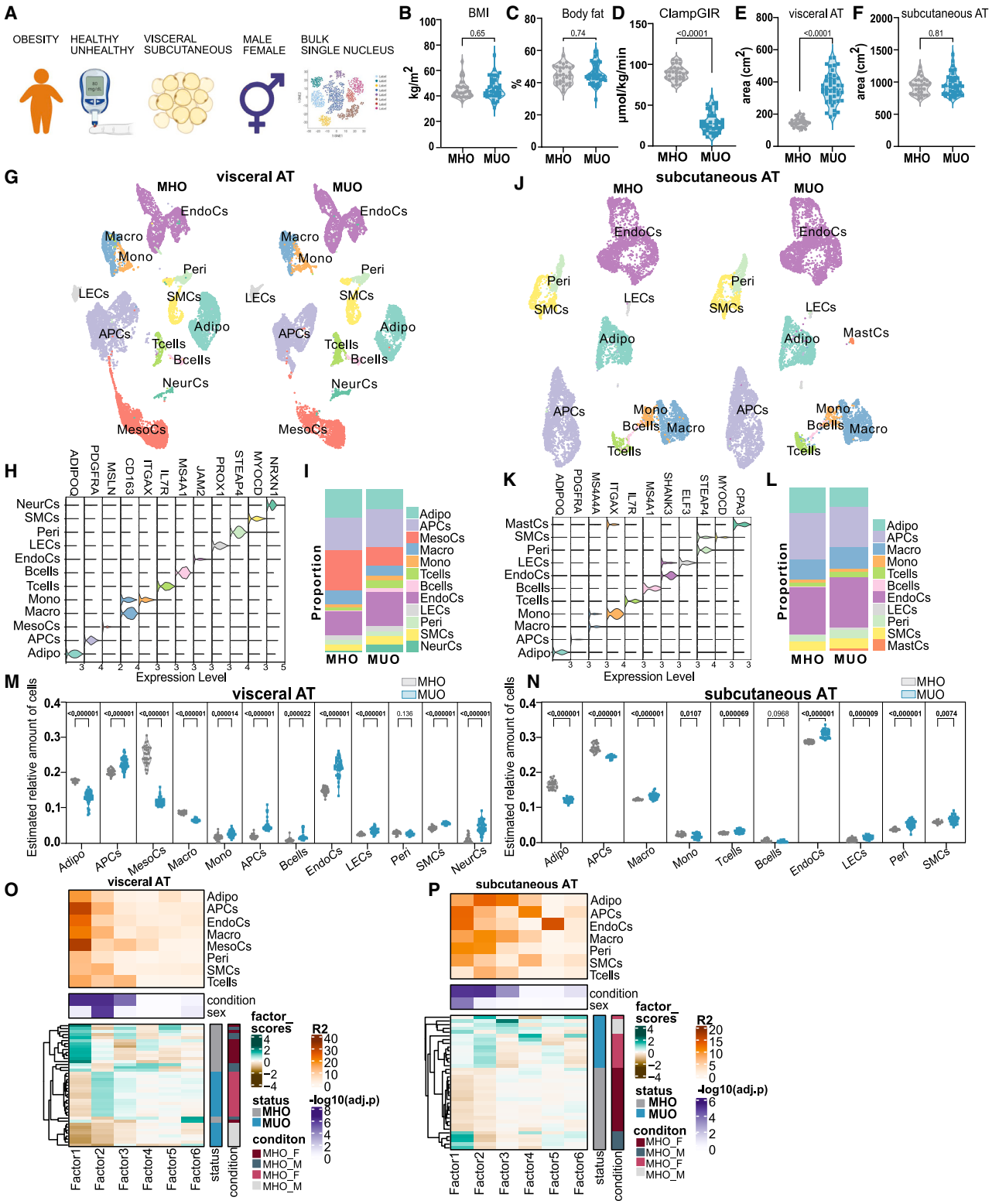

Figure 1. Adipose tissue of individuals with obesity is extensively remodeled in different health states in a depot-specific manner

(A) Cohort design and experimental plan.

(B–F) (B) BMI, (C) body fat, (D) euglycemic, hyperinsulinemic clamp glucose infusion rate (ClampGIR), (E) visceral, and (F) subcutaneous AT area distribution between individuals with MHO (n = 32) and MUO (n = 45).

(legend continued on next page)

Please cite this article in press as: Reinisch et al., Unveiling adipose populations linked to metabolic health in obesity, Cell Metabolism (2024), https://doi.org/10.1016/j.cmet.2024.11.006

influence AT function and metabolic health, such as adipose topography, adiposity, and gender. Combining the cell-type-specific information with bulk transcriptomics of AT samples, and clinical parameters, we identified key players for unhealthy AT remodeling and AT-specific predictors for metabolic disease risk. Based on these datasets, future studies can identify novel, cell-type-specific biomarkers to assess AT function, thus providing a roadmap for more phenotype-tailored options in obesity treatment.

RESULTS

AT of individuals with obesity is extensively remodeled in different health states in a depot-specific manner

To study the involvement of AT function in metabolic disease, we collected clinical parameters, and white subcutaneous and visceral AT samples in a cohort of 77 men and women with MHO and MUO and performed bulk- and single-nucleus (sn) RNA sequencing (Figure 1A). Individuals with MHO had similar body mass index (BMI) (Figure 1B), body fat content (Figure 1C), body weight, and waist circumference compared to individuals with MUO (Tables 1 and S1) but were characterized by significantly better markers for insulin sensitivity (glucose infusion rate during the steady state of an euglycemic-hyperinsulinemic clamp (Figure 1D), fasting plasma glucose and insulin, oral glucose tolerance), lipid homeostasis (fatty acids, high-density lipoprotein [HDL] cholesterol) and liver function tests (ALAT and ASAT, all Table S1). As previously described,[4] individuals with MUO showed a striking increase in visceral AT (Figure 1E) area, whereas the amount of subcutaneous AT was unchanged (Figure 1F).

The strong differences in intra-abdominal adiposity among the study participants provided the ideal framework to investigate mechanisms of unhealthy AT remodeling and their potential role in disease development. Thus, we performed bulk RNA sequencing of both depots from individuals with MHO and MUO. Unexpectedly, despite a clear separation by systemic metabolic parameters, the WAT transcriptome of MHO and MUO did not separately cluster in the two-dimensional principal-component analysis (PCA) space (Figures S1A and S1B). In line with a large heterogeneity in the dataset, the metabolic-health-associated differences in the bulk transcriptomic profile were subtle, as validated by few differentially expressed genes with 2-fold change in visceral AT ($n = 120$, $p < 0.01$) and subcutaneous ($n = 19$, $p < 0.01$) AT comparing MUO against MHO (Figures S1C and S1D).

As AT harbors the capacity to flexibly adapt its cellular composition under physiological and pathological conditions,[10] we hypothesized that transcriptional differences might be masked by alterations in the cellular profile of AT. Thus, we performed snRNA sequencing of pooled AT samples (Tables S2 and S3) from each depot of individuals with MHO and MUO. We were able to retrieve 28,931 nuclei for visceral and 19,186 nuclei for subcutaneous AT after quality filtering and annotated all broad canonical cell populations present in AT based on previously described markers[11] (Figures 1G, 1H, 1J, 1K, S1E, and S1F). The cellular composition of visceral AT was remarkably different comparing MHO with MUO, affecting the abundance of almost every cell population (Figures 1G and 1I), whereas the cellular landscape of subcutaneous AT was mostly unchanged (Figures 1J and 1L). The most prominent changes were evident by an overrepresentation of the relative proportion of mesothelial cells (MesoCs) in visceral AT of individuals with MHO (Figures 1G and 1I). Furthermore, the fraction of visceral adipocytes was higher in MHO over MUO (Figures 1G and 1I) indicative of maintained adipocyte hyperplasia.

To preserve individual AT heterogeneity often masked by pooling, we demultiplexed the snRNA-sequencing datasets based on called SNPs (Figures S1G and S1H). We found that the compositional differences of visceral AT between the conditions remained consistent across the SNP-demultiplexed individuals, reinforcing the reliability of our dataset (Figure S1G). To further extend our observation and increase statistical power, we deconvoluted the bulk RNA-sequencing dataset of the whole cohort, using cell-type-specific markers identified by snRNA sequencing. We again confirmed that changes in the above-mentioned populations of visceral AT were conserved (Figure 1M). Additionally, by deconvoluting the bulk RNA-sequencing dataset of subcutaneous AT, we were able to capture significant changes in the relative abundance of several cell populations comparing MHO and MUO (Figure 1N). Most notably, the estimated relative abundance of adipocytes and adipocyte-progenitor cells (APCs) was higher in MHO compared to MUO in subcutaneous AT (Figure 1N).

(G) Uniform manifold approximation and projection (UMAP) of 28,931 nuclei representing visceral AT from 41 pooled individuals with MHO and MUO colored by broad cell types.
(H) Violin plot showing selected marker gene expression for visceral AT cell clusters.
(I) Bar plots showing relative cell-type proportions in visceral AT of individuals with MHO and MUO.
(J) UMAP of 19,186 nuclei representing subcutaneous AT of pooled 36 individuals with MHO and MUO colored by broad cell types.
(K) Violin plot showing selected marker gene expression for subcutaneous AT cell clusters.
(L) Bar plots showing relative cell-type proportions in subcutaneous AT of individuals with MHO and MUO.
(M and N) Violin plots showing estimated relative cell-type proportions from the bulk RNA-sequencing deconvolution of (M) visceral and (N) subcutaneous AT of individuals with MHO ($n = 31, 29$) and MUO ($n = 43, 39$) based on the marker genes identified by snRNA sequencing.
(O and P) Multi-cellular factor analysis summary for (O) visceral and (P) subcutaneous AT showing the hierarchical clustering of latent factor scores across the pooled individuals as inferred by the model. Percentage of explained variance (R^2) by each indicated cell type and statistical associations (adjusted p values from ANOVA) with covariates (condition, sex) are shown for each latent factor in the upper panel. Condition and status of each SNP-demultiplexed individual are indicated in the lower panel.
Statistical significance was analyzed by Wilcoxon signed-rank test (B–F), two-tailed unpaired t test (M–N) or one-way ANOVA with Tukey post hoc tests (O and P). (Abbreviations: adipose tissue, AT; metabolically healthy obesity, MHO; metabolically unhealthy obesity, MUO; adipocytes, Adipo; adipocyte-progenitor cells, APCs; mesothelial cells, MesoCs; endothelial cells, EndoCs; lymphatic endothelial cells, LECs; macrophages, Macro; monocytes, Mono; pericytes, Peri; smooth muscle cells, SMCs; neuronal like cells, NeurCs; and mast cells, MastCs).

Please cite this article in press as: Reinisch et al., Unveiling adipose populations linked to metabolic health in obesity, Cell Metabolism (2024), https://doi.org/10.1016/j.cmet.2024.11.006

Table 1. Summary of key clinical parameters characterizing individuals with MHO and MUO

Parameters	MHO (n = 32)	MUO (n = 45)	FDR
Sex (female/male)	23/9	32/13	N/A
Adiponectin (μg/mL)	6.93 ± 3.39	3.24 ± 1.77	<0.0001
Age (years)	38.75 ± 10.98	47.09 ± 7.49	0.002
BMI (kg/m^2)	46 ± 6.82	46.89 ± 8.12	0.65
Body fat (%)	44.72 ± 5.6	45.55 ± 6.48	0.74
Clamp GIR (μmol/kg/min)	89.38 ± 9.05	29.36 ± 12.5	<0.0001
FPG (mmol/L)	5.22 ± 0.19	5.67 ± 0.34	<0.0001
FPI (pmol/L)	28.74 ± 14.17	107.96 ± 30.32	<0.0001
Free fatty acids (mmol/L)	0.23 ± 0.15	0.47 ± 0.2	<0.0001
gGT (μkat/L)	0.4 ± 0.18	0.63 ± 0.34	0.0001
HbA1c (%)	5.28 ± 0.15	5.81 ± 0.37	<0.0001
Insulin stimulated glucose transport (pmol/mg/min)	5.02 ± 1.14	2.24 ± 0.71	<0.0001
Subcutaneous fat area (cm^2)	932.13 ± 124.48	953.67 ± 161.15	0.81
Visceral fat area (cm^2)	133.41 ± 24.07	343.78 ± 94.37	<0.0001
Waist circumference (cm)	141.63 ± 13.01	141.96 ± 15.31	0.91
Weight (kg)	134.99 ± 21.07	134.25 ± 27.85	0.81

Values are shown as mean ± SD. FDR was calculated based on Wilcoxon signed-rank test. (Abbreviations: body mass index, BMI; glucose infusion rate, GIR; fasting plasma glucose, FPG; fasting plasma insulin, FPI; gamma-glutamyl transferase, gGT; and glycated hemoglobin A1c, HbA1c).

In line with the subtle compositional differences in subcutaneous AT, correlating the estimated relative amount of adipose populations with metabolic markers revealed that visceral populations were strongly associated with metabolic disease, (Figure S1I), whereas subcutaneous AT showed weaker associations (Figure S1J). Specifically, in visceral AT, MesoCs and adipocytes demonstrated robust positive correlations with a favorable metabolic profile (Figure S1I). To explore the single-nuclei datasets in an unsupervised manner, we performed multi-cellular factor analysis (MOFA-cell[15]). We restricted the analysis only to the well represented major cell types across the SNP-demultiplexed individuals to capture the principal source of variation (Figures 1O and 1P). For visceral AT, results showed a clear conditional separation between MHO and MUO captured by all the factor scores (Figure S1K), but most strongly along latent factor 1 (Figure S1L), which is predominantly driven by the transcriptional differences in MesoCs and APCs (Figure 1O). In contrast to visceral AT, the conditional separation of subcutaneous AT was less pronounced, as captured by all factor scores (Figure S1M). Nevertheless, we still observed conditional separation between MHO and MUO (Figure S1N) along subcutaneous latent factor 2, mainly driven by the transcriptional differences in adipocytes (Figure 1P). Overall, MesoCs and APCs were able to individually explain more than 50% of the transcriptional variability in the visceral AT snRNA-seq dataset (Figure S1O), whereas adipocytes individually explained about 30% of the transcriptional variability in subcutaneous AT (Figure S1P).

Together, we generated the first cellular-resolved map capturing the transcriptional differences in visceral and subcutaneous AT of MHO and MUO, thereby identifying AT-specific cell types that are most strongly associated with metabolic health.

AT compositional changes in individuals with MUO are predominantly independent of sex and adiposity

A significant amount of literature suggests that there is a sex dimorphism in the susceptibility to develop metabolic disease upon obesity progression.[16] In line, MOFA-cell revealed that latent factor 2 in visceral AT clearly separates the transcriptome of women and men (Figure 1O). This factor was mainly driven by APCs and macrophages (Figure 1O), and the conditional separation by sex was only evident in MUO, not in MHO (Figures 2A and 2B). In subcutaneous AT, sex introduced even more variation in the dataset than metabolic health (Figure 1P). Factor 1 was decisive for the sex-dependent conditional separation in MHO (Figure S2A), which was driven by transcriptional differences in APCs and EndoCs (Figure 1P), and adipocyte-driven factor 3 conditionally separated women and men with MUO (Figure S2B).

On a systemic level, stratifying plasma parameters by sex revealed subtle difference in disease severity, with women in general being more insulin sensitive (Figures 2C–2E), despite no differences in overall adiposity (Figure S2C), waist circumference (Figure S2D), or plasma lipid parameters and HbA1c levels (Figures S2E–S2I). The subcutaneous AT volume was unchanged (Figure 2F), whereas visceral AT volume (Figure 2G) and body weight (Figure S2J) of men with MUO was significantly higher compared with women with MUO. Interestingly, women with MUO were significantly older than women with MHO (Figure S2K), which is in line with unfavorable AT distribution and metabolic disease development in post-menopausal women.[16]

Given the strong sex-dependent conditional separation of individuals with MUO, we stratified the snRNA sequencing and deconvoluted bulk RNA-sequencing datasets of MUO by sex (Figures 2H–2M).

Despite subtle changes in the disease-induced alterations in the cellular composition of visceral (Figures 2H, 2I, and S2L) and subcutaneous AT (Figures 2J, 2K, and S2M) in the pooled

Please cite this article in press as: Reinisch et al., Unveiling adipose populations linked to metabolic health in obesity, Cell Metabolism (2024), https://doi.org/10.1016/j.cmet.2024.11.006

CellPress
OPEN ACCESS

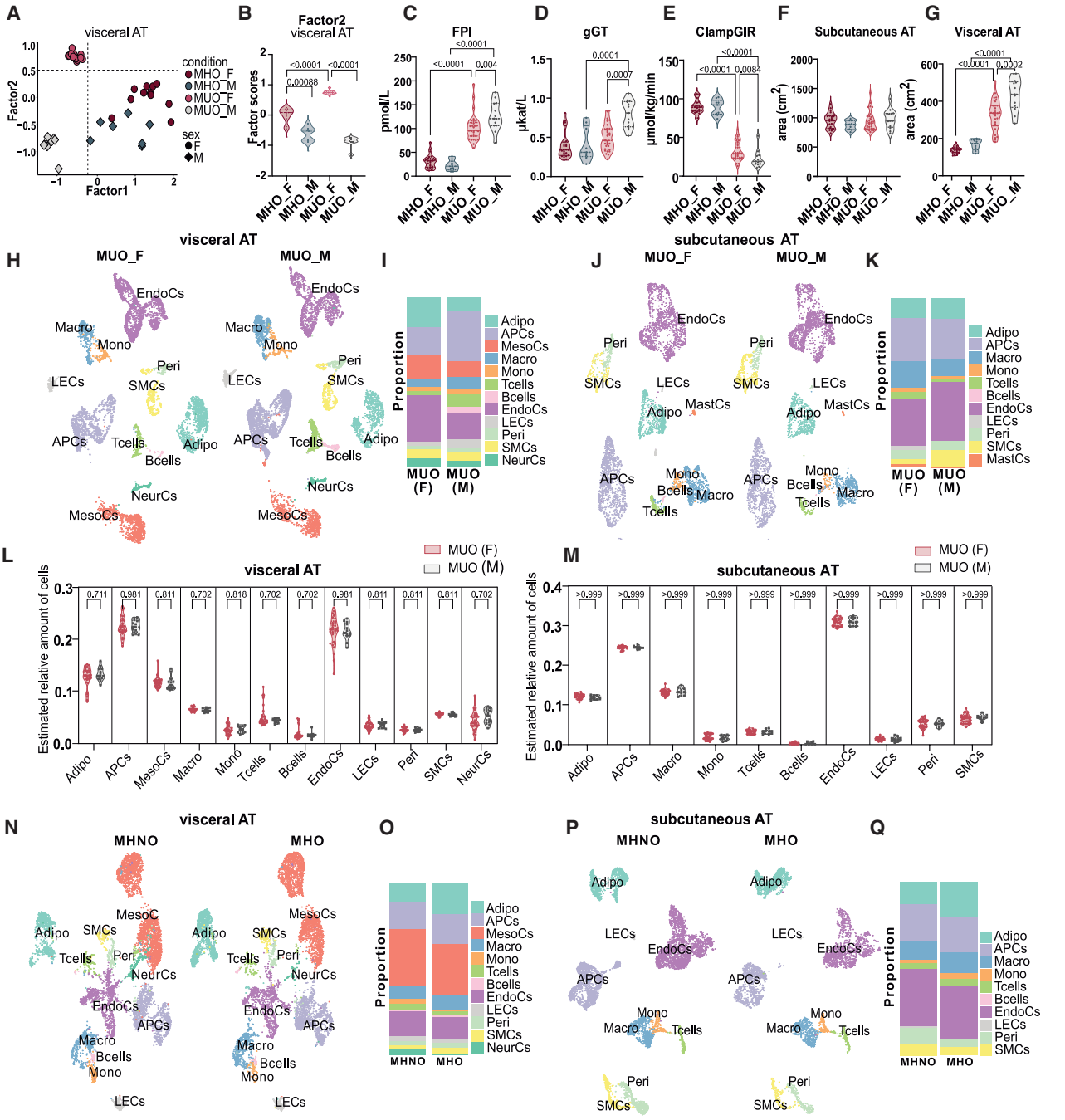

Figure 2. AT compositional changes in visceral AT of MHUO are mostly independent of sex and adiposity

(A) Multi-cellular factor analysis showing the separation of MHO and MUO or male and female within MUO, respectively, along the visceral AT latent factors 1 and 2.

(B) Violin plot showing visceral AT latent factor 2 score distribution in male (_M) and female (_F) individuals with MHO and MUO.

(C–G) (C) Fasting plasma insulin (FPI), (D) glucose tolerance (gGT), (E) euglycemic, hyperinsulinemic clamp glucose infusion rate (ClampGIR), (F) subcutaneous, and (G) visceral AT area distribution across female (_F) and male (_M) individuals with MHO or MUO.

(H and J) UMAPs representing (H) visceral and (J) subcutaneous AT (13,882 and 10,354 nuclei, respectively) of individuals with MUO (n = 23) colored by broad cell types.

(I and K) Bar plots showing relative cell-type proportions in (I) visceral and (K) subcutaneous AT of individuals with MUO, split by sex.

(L and M) Violin plots showing estimated relative cell-type proportions from the bulk RNA-sequencing deconvolution of (L) visceral and (M) subcutaneous AT of individuals with MUO (n = 43, 39), split by sex.

(N and P) UMAPs representing (N) visceral and (P) subcutaneous AT (14,349 and 10,117 nuclei, respectively) of metabolically healthy non-obese (MHNO) individuals and individuals with MHO (n = 13) colored by broad cell types.

(legend continued on next page)

Please cite this article in press as: Reinisch et al., Unveiling adipose populations linked to metabolic health in obesity, Cell Metabolism (2024), https://doi.org/10.1016/j.cmet.2024.11.006

snRNA-sequencing dataset, the estimated proportion of cell types derived from the deconvoluted bulk RNA-sequencing datasets did not show statistically significant changes between sexes (Figures 2L and 2M), suggesting that these alterations are not conserved in a larger group of individuals.

Next, we aimed to investigate whether high adiposity per se, without increased metabolic disease parameters, induces tissue remodeling. Therefore, we performed snRNA sequencing on pooled AT samples of each depot from an independent cohort of non-obese, metabolically healthy (MHNO) individuals (clinical data summary in Table S4), Interestingly, we could not find major cellular compositional differences in visceral (Figures 2N and 2O) or subcutaneous AT (Figures 2P and 2Q) when comparing the composition of MHNO with MHO, reinforcing that healthy AT expansion is strongly linked to preserved systemic nutrient homeostasis despite obesity. The only differences we found in both depots were a higher number of adipocytes in the obese compared with non-obese group, but this did not reach statistical significance upon demultiplexing of the snRNA-seq datasets (Figures S2N and S2O).

Together, MOFA-cell analysis revealed transcriptional differences in distinct cell types comparing women and men with MUO, which might explain the sex-based dimorphism in the severity of metabolic disease. However, the broad compositional changes induced by unhealthy AT remodeling were mainly independent of sex and adiposity.

Adipocyte function is strongly associated with metabolic health

Adipocytes are among the first responders to nutritional cues and metabolic flexibility of adipocytes is crucial for AT function.[17] Furthermore, recent studies have begun to dissect adipocyte heterogeneity within a single adipose depot, suggesting that they can be stratified into several distinct subpopulations.[11–13,18]

In line with previous data,[4] we found that the maximal and mean adipocyte size was significantly higher in the metabolically unhealthy group (Figure 3A). Furthermore, we identified a marked cellular heterogeneity of adipocytes, which is demonstrated by clustering of visceral adipocytes into five populations (vAdipo1-5) (Figures 3B and 3C). By performing a detailed comparison of the gene signature of the five subclusters with previously defined adipocyte subpopulations, we found that Adipo1 (leptin [LEP]), Adipo2 (perilipin [PLIN]), and Adipo3 (serum amyloid A1 [SAA1]) (Figure 3B), correspond to the three white adipocyte subtypes identified by Bäckdahl et al.[13] (Figure S3A). These subclusters showed an enrichment of inflammatory (Adipo1 [LEP], Figure S3B), lipid-metabolic (Adipo2 [PLIN], Figure S3C), and adipogenic (Adipo3 [SAA1], Figure S3D) pathways. Two adipocyte subpopulations were unique to the visceral depot, namely vAdipo4 (fibroblast growth factor 14 [FGF14]) and vAdipo5 (fms-like tyrosin linase 1 [FLT1]) (Figures 3B and 3C), which were characterized by an upregulation of pathways involved in focal adhesion (Figure S3E) and angiogenic pathways (Figure S3F), respectively. Unexpectedly, the systemic health state did not affect the prevalence of any visceral adipocyte subpopulation (Figures 3D and S3G–S3I).

To further compare Adipo1-5 with previously published datasets, we projected our visceral subclusters onto the dataset of Emont et al.[11] We noted that most adipocyte subpopulations were predicted to be hAd2 in visceral AT (Figure S5J), which were described as visceral-specific basal adipocytes.[11] To investigate similarities of the two datasets on a more holistic level, we compared adipocyte-specific enriched pathways and found that vAdipo4 (FGF14) corresponded to the thermogenic, axon-guidance-enriched hAd6 population, and vAdipo5 showed a stronger enrichment of antigen-presenting pathways like hAd2 (Figure S3K).[11]

To examine the coherence in how adipocytes respond to metabolic health conditions, we performed pseudobulk analysis using SNP-demultiplexed individuals and visualized visceral adipocytes in the two-dimensional PCA space. In contrast to the lack of conditional separation in the bulk RNA-sequencing data, the snRNA-seq data revealed a clear separation between visceral adipocytes from healthy and diseased conditions (Figure 3E). In line with numerous studies, which reported that adipocyte hypertrophy induces metabolic inflexibility (as reviewed in e.g., Blüher[19]), we found a decreased abundance of transcripts encoding for metabolic pathways (Figure 3F) and a significant enrichment of genes involved in hypoxia-related pathways (Figure 3G) when comparing metabolically unhealthy over healthy visceral adipocytes.

Next, we focused our analysis on adipocytes from the subcutaneous AT depots. Re-clustering of subcutaneous adipocytes led to the identification of two depot-specific populations, sAdipo4 (early growth response 1 [EGR1]) and sAdipo5 (neuronal-related cell adhesion molecule [NRCAM]), whereas Adipo1–3 were conserved among visceral and subcutaneous AT (Figures 3H, 3I, and S4A). Interestingly, the relative proportion of sAdipo5 (NRCAM) was strongly and consistently higher in subcutaneous AT of MUO compared with MHO (Figures 3J, 3K, S4B, and S4C). The subcutaneous-specific adipocyte subpopulations were characterized by the enrichment of genes involved in inflammation-related pathways (sAdipo4 [EGR1], Figure S4D), and growth-related pathways, such as mitogen-activated protein kinase (MAPK) signaling (sAdipo5 [NRCAM], Figure 3L). By comparing adipocytes of the Emont et al. dataset with our subcutaneous adipocyte subclusters, we noted that most of the adipocyte subpopulations were predicted to be hAd1 (Figure S4E), which represent subcutaneous-specific basal adipocytes.[11] More detailed analysis revealed that sAdipo4 (EGR1) shared similarities with the gene signature of hAd1, and sAdipo5 (NRCAM) and sAdipo3 (SAA1) exhibited an enrichment of pathways involved unsaturated fatty acid synthesis like hAd4 (Figure S4F).[11]

In line with the disease-dependent transcriptional alterations in visceral adipocytes, we found that the transcriptome of

(O and Q) Bar plots showing relative cell-type proportions in (O) visceral and (Q) subcutaneous AT of MHNO and MHO.
Statistical significance was analyzed by one-way (B) and two-way ANOVA (C–G) with Tukey post hoc tests or by two-tailed unpaired t test (L and M). (Abbreviations: adipose tissue, AT; metabolically healthy obesity, MHO; metabolically unhealthy obesity, MUO; metabolically non-healthy obese, MHNO; adipocytes, Adipo; adipocyte-progenitor cells, APCs; mesothelial cells, MesoCs; endothelial cells, EndoCs; lymphatic endothelial cells, LECs; macrophages, Macro; monocytes, Mono; pericytes, Peri; smooth muscle cells, SMCs; neuronal like cells, NeurCs; and mast cells, MastCs).

Please cite this article in press as: Reinisch et al., Unveiling adipose populations linked to metabolic health in obesity, Cell Metabolism (2024), https://doi.org/10.1016/j.cmet.2024.11.006

CellPress
OPEN ACCESS

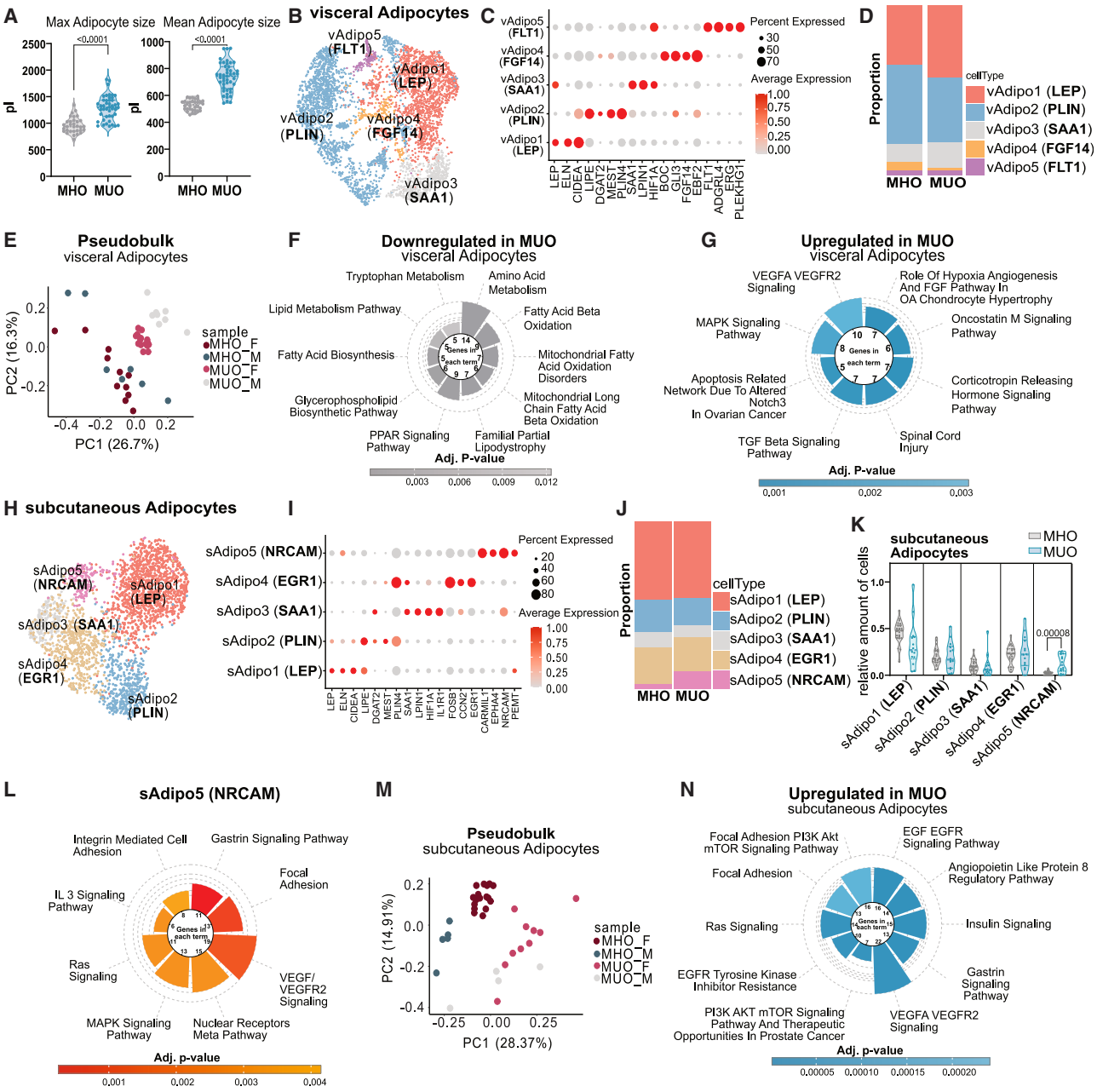

Figure 3. Adipocyte function is strongly associated with metabolic health

(A) Maximal and mean visceral adipocyte size distribution in individuals with MHO and MUO.
(B) UMAP of 4,375 nuclei representing visceral adipocytes of individuals with MHO and MUO.
(C) Dot plot showing expression of marker genes used for annotating visceral adipocyte subpopulations.
(D) Bar plots showing relative proportions of visceral adipocyte subpopulations in MHO and MUO.
(E) PCA of pseudobulk data from SNP-demultiplexed individuals showing cluster formation of visceral adipocytes between MHO and MUO, split by sex.
(F and G) Top significant (F) downregulated and (G) upregulated WikiPathways in visceral adipocytes of individuals with MUO vs. MHO.
(H) UMAP of 2,614 nuclei representing subcutaneous adipocytes of individuals with MHO and MUO.
(I) Dot plot showing expression of marker genes used for annotating subcutaneous adipocyte subpopulations.
(J) Bar plots showing relative proportions of subcutaneous adipocyte subpopulations in MHO and MUO.
(K) Violin plots showing relative subcutaneous adipocyte subtype proportions of SNP-demultiplexed individuals with MHO and MUO.
(L) Most significantly enriched WikiPathways of subcutaneous adipocyte subpopulation 5 (sAdipo5 [NRCAM]) based on top marker genes.
(M) PCA of pseudobulk data from SNP-demultiplexed individuals showing cluster formation of subcutaneous adipocytes between MHO and MUO, split by sex.
(N) Top significant upregulated WikiPathways in subcutaneous adipocytes of individuals with MUO vs. MHO.
Statistical significance was analyzed by two-tailed unpaired t test (A and K). (Abbreviations: visceral adipocytes, vAdipo and subcutaneous adipocytes, sAdipo).

Please cite this article in press as: Reinisch et al., Unveiling adipose populations linked to metabolic health in obesity, Cell Metabolism (2024), https://doi.org/10.1016/j.cmet.2024.11.006

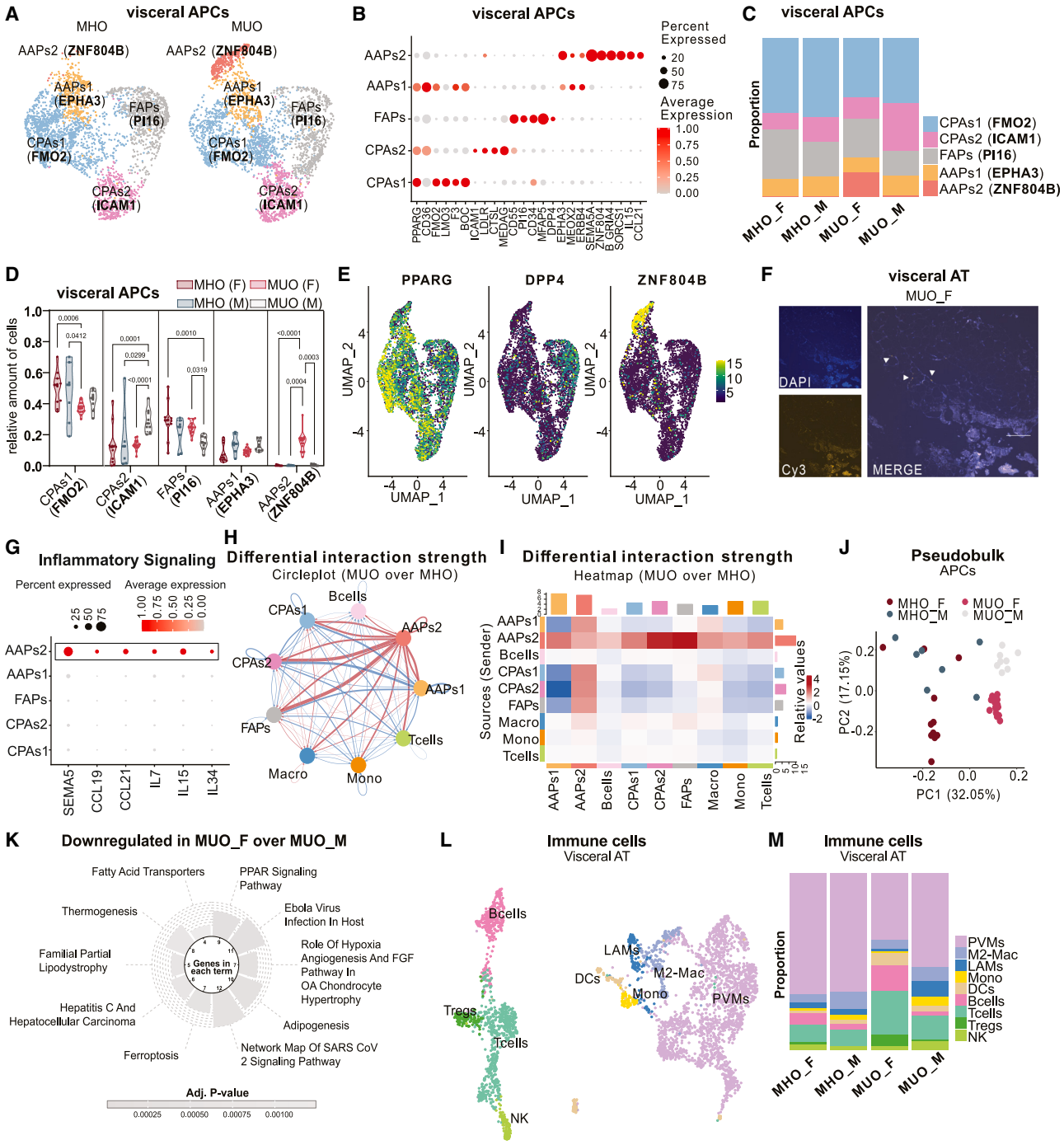

Figure 4. snRNA sequencing uncovers a woman-specific, highly secretory anti-adipogenic progenitor population that might recruit adaptive immune cells to visceral AT

(A) UMAP of 6,233 nuclei representing visceral APCs of individuals split by MHO and MUO.

(B) Dot plot showing expression of marker genes used for annotating visceral APC subpopulations.

(C) Bar plots showing relative proportions of visceral APCs in MHO and MUO, split by sex.

(D) Violin plots showing relative visceral APC subtype proportions of SNP-demultiplexed individuals with MHO and MUO, split by sex.

(E) Feature plots showing expression of *PPARG*, *DPP4*, and *ZNF804B* in visceral APCs.

(F) RNA-scope based staining showing *in situ* hybridization of probes for ZNF804B in visceral AT of a woman with MUO.

(G) Dot plot showing expression (indicated by color) of cytokines in visceral APCs.

(H and I) (H) Circle plot and (I) heatmap showing predicted differential strength of cell-cell interactions for the indicated sub populations with color indicating increased (red) or decreased (blue) signaling in visceral AT of MUO vs. MHO.

(J) PCA of pseudobulk data from SNP-demultiplexed individuals showing cluster formation of visceral APCs between MHO and MUO, split by sex.

(legend continued on next page)

Please cite this article in press as: Reinisch et al., Unveiling adipose populations linked to metabolic health in obesity, Cell Metabolism (2024), https://doi.org/10.1016/j.cmet.2024.11.006

subcutaneous adipocytes derived from the snRNA-seq datasets is clearly separable between MHO and MUO (Figure 3M). Interestingly, we found that the transcript abundance of genes mapping to insulin signaling pathways was increased in subcutaneous adipocytes of MUO (Figure 3N).

Taken together, we confirmed that different adipocyte states/subpopulations exist, with only one subcutaneous adipocyte subcluster being enriched in the disease state. Furthermore, we illustrated that visceral adipocyte subpopulations consistently transition from a metabolically active to a hypoxic phenotype.

snRNA sequencing uncovers a woman-specific, highly secretory anti-adipogenic progenitor population that might recruit adaptive immune cells to visceral AT

Adipocyte hypertrophy and AT remodeling in MUO individuals is facilitated by the interaction of different cell populations in their respective niche.[17] Among them, APCs serve as a source of new adipocytes upon obesity progression, and more recent publications reported that they can control the pro-inflammatory phenotype of AT under disease conditions (as reviewed in, e.g., Ferrero et al.[20]).

To analyze APC heterogeneity and function under MHO and MUO, we re-clustered the APCs, allowing us to stratify them into five different visceral (Figures 4A and 4B) and four subcutaneous populations (Figures S5A and S5B), all of which express platelet-derived growth factor receptor alpha (*PDGFRA*) and laminin subunit alpha 2 (*LAMA2*) (Figures S5C and S5D). Based on the published markers,[10] we defined them as fibro-adipogenic progenitors (FAPs), anti-adipogenic progenitors (AAPs), and two distinct committed preadipocyte populations (CPAs1 and CPAs2; Figures S5E and S5F). In visceral AT, AAPs were further clustered into two subpopulations, AAPs1 (*EPHA3*+ *ZNF804B*−), and AAPs2 (*EPHA3*+ *ZNF804B*+; Figures 4A and 4B). The abundance of subcutaneous APC subpopulations was unchanged among the groups (Figures S5G and S5H), whereas many of the visceral APC subpopulations showed dependency on metabolic health status, sex, or both (Figures 4C and 4D). In detail, CPAs1 (flavin-containing monooxygenase 2 [FMO2]) were decreased in visceral AT of MUO (Figures 4C and 4D). In contrast, the relative abundance of CPAs2 (intercellular adhesion molecule 1 [ICAM1]) was increased in men with MUO, but not in women, which inversly correlated with the abundance of FAPs (Figures 4C and 4D). Both CPAs highly expressed adipogenic genes like peroxisome proliferator-activated receptor gamma (*PPARG*, Figure 4E), in line with their advanced commitment along the adipogenic trajectory, and FAPs expressed the stem cell marker dipeptidyl-peptidase 4 (*DPP4*, Figure 4E). The most prominent changes were reflected by an increase in a visceral-specific subpopulation defined as AAPs2 in MUO (Figures 4C and 4D), which was characterized by the expression of zinc finger protein 804B (*ZNF804B*) (Figure 4E). We detected ZNF804B-positive cells within the crown-like structures of visceral AT of a woman with MUO (Figure 4F). Interestingly, the increased relative abundance of AAPs2 (ZNF804B) was strongly sex dependent as we could not detect this progenitor population in men with obesity of any group (Figures 4C and 4D). Furthermore, ZNF804B was captured among the significantly differentially expressed genes comparing visceral APCs of women and men with MUO (Figure S6A), and as one of the strongest markers separating sexes in MUO in MOFA-cell visceral AT factor 2. Transcriptional signature analysis of AAPs2 (ZNF804B) revealed that they selectively expressed several cytokines (Figure 4G). In line, ligand-receptor interaction analysis confirmed that AAPs2 had a high secretory capacity and interacted with other APC subpopulations and immune cells (Figure 4H). These interactions were notably enriched in visceral AT of MUO (Figures 4H and 4I), which was mainly mediated by an increase in pathways that affect immune cell recruitment or extra-cellular matrix composition (like PTPRC, THBS1, and LAMA3 signaling, Figure S6B).

We next investigated whether AAPs2 could inhibit adipogenesis in a sex-specific way. The transcriptional signature of APCs is clearly separating men and women with MUO (Figure 4J), and adipogenic pathways such as PPARG signaling are globally downregulated in APCs of women with MUO compared with men with MUO (Figure 4K). Additionally, the predicted interaction of AAPs2 with immune cells as well as their high expression of genes encoding for cytokines prompted us to investigate if the abundance of this population correlates with the number of immune cells in visceral AT. Re-clustering the visceral immune cell populations (Figures 4L and S6C) revealed that the relative abundance of T regulatory cells (Tregs), B cells, and dendritic cells (DCs) was higher in visceral AT of MUO compared with MHO (Figures 4L, 4M, S6C, and S6D). Interestingly, this enrichment of adaptive immune cells was only present in MUO women, but not men (Figures 4M and S6E), which corresponded to the presence of AAPs2 (ZNF804B). Additionally, PVMs and LAMs were overrepresented in men with MUO compared with women with MUO, consistent with an overall increase in macrophage numbers as validated by immunohistochemistry (Figure S6F). In contrast to visceral AT, the immune cell subtypes in subcutaneous AT did not change in response to metabolic health or sex (Figures S6G–S6J).

Taken together, we describe a so far unrecognized potential crosstalk between an inflammatory, visceral-specific AAP population and adaptive immune cells in women with MUO.

Transitioning of MesoCs along the epithelial to mesenchymal state strongly correlates with metabolic health

MesoCs have so far been regarded as an inert cell population, which forms a protective layer surrounding AT in the visceral compartment.[21] However, more recent studies revealed a great

(K) Top significant downregulated WikiPathways in visceral APCs of MUO female vs. male.
(L) UMAP of 3,710 nuclei representing visceral immune cells of individuals colored split by MHO and MUO.
(M) Bar plots showing relative proportions of visceral immune cell subpopulations in MHO and MUO, split by sex.
Statistical significance was analyzed by two-way ANOVA with Tukey post hoc tests (D). (Abbreviations: adipocyte-progenitor cells, APCs; anti-adipogenic progenitors, AAPs; fibro-adipogenic progenitors, FAPs; committed pre-adipocytes, CPAs; perivascular macrophages, PVMs; M2-macrophages, M2-Mac; lipid-associated macrophages, LAMs; monocytes, Mono; dendritic cells, DCs; natural killer cells, NK; and T regulatory cells, Tregs).

Please cite this article in press as: Reinisch et al., Unveiling adipose populations linked to metabolic health in obesity, Cell Metabolism (2024), https://doi.org/10.1016/j.cmet.2024.11.006

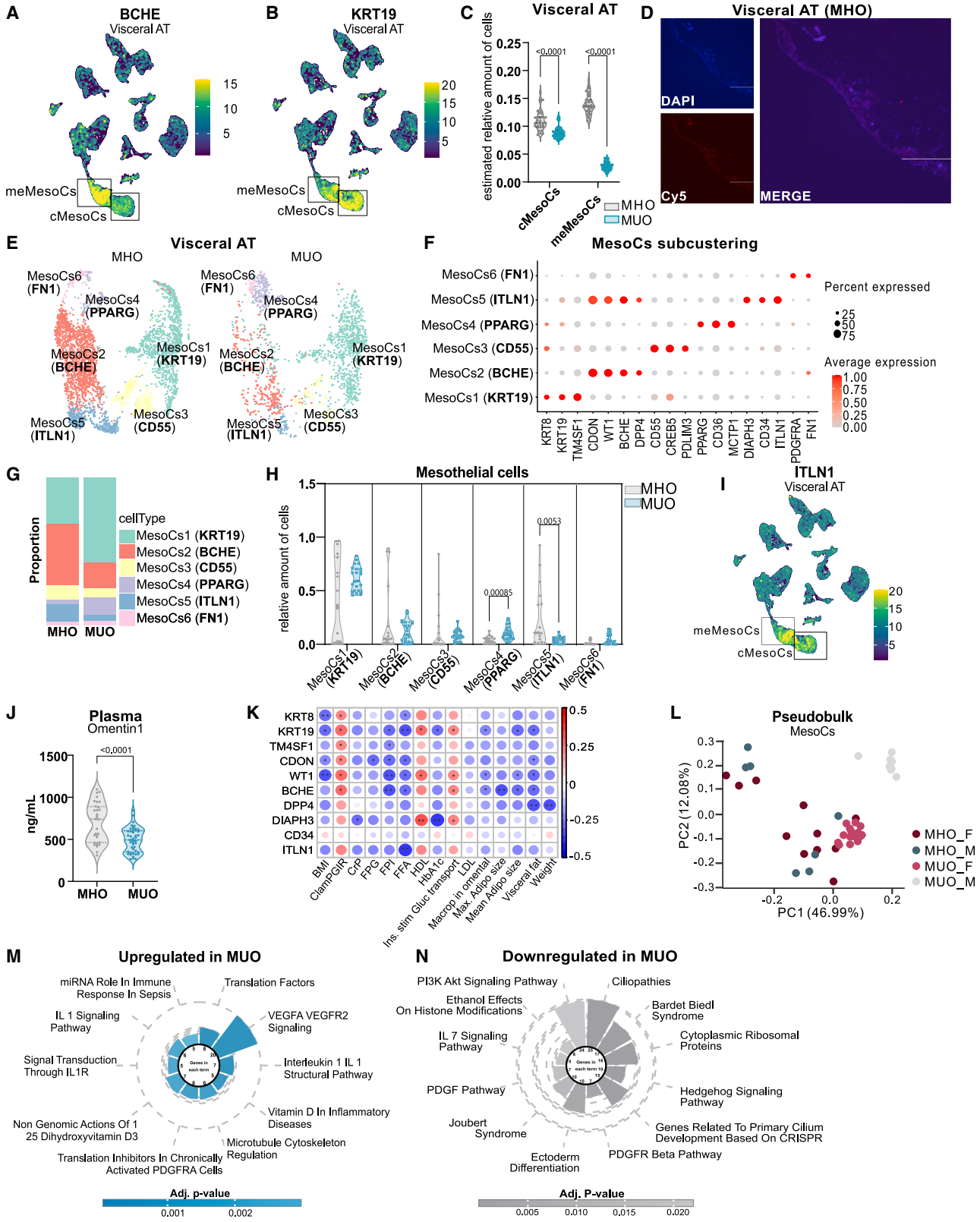

(legend on next page)

Please cite this article in press as: Reinisch et al., Unveiling adipose populations linked to metabolic health in obesity, Cell Metabolism (2024), https://doi.org/10.1016/j.cmet.2024.11.006

cellular heterogeneity of MesoCs[11,12] and pointed to a potential transition of MesoCs to the mesenchymal state.[14]

In line, we noted that MesoCs of the broad clustering separated into two distinct populations, of which one was characterized by the expression of *BCHE* (Figure 5A), while both populations expressed the MesoC marker *KRT19* (Figure 5B). The BCHE-positive mesothelial subpopulation showed a dual gene expression signature, as indicated by the increased expression of genes involved in mesenchymal programs (such as *CDON* and *BCHE*; Figure S7A); thus, we defined them as mesenchymal MesoCs (meMesoCs). Interestingly, we found a notably stronger enrichment of meMesoCs in MHO over MUO compared with classical MesoCs (cMesoCs) by deconvoluting the bulk dataset (Figure 5C). In line, stratifying the MesoCs in these two broad populations revealed that meMesoCs showed a stronger positive correlation with several systemic parameters of metabolic health (Figure S7B). Next, we examined the anatomical location of these cells by *in situ* hybridization using RNA-scope. There, BCHE-positive cells were mainly located at the boundaries of AT lobules but can also be partly found interspersed in AT, surrounding adipocytes (Figure 5D).

Considering the high similarities of meMesoCs with APCs, we compared the transcriptional signature of the MesoCs with previously published datasets of visceral AT.[11,12,14] MesoCs exclusively expressed mesothelial markers (Figure S7C), with meMesoCs also expressing mesenchymal markers (Figure S5D). APCs lacked expression of MesoCs markers *KRT19*, *TM4SF1*, and *EZR*, distinguishing meMesoCs from classical adipogenic progenitors (Figure S7D).

Re-clustering of cMesoCs and meMesoCs revealed six different subpopulations that flexibly change in their abundance comparing MHO with MUO (Figures 5E and 5F). All MesoCs subclusters, besides MesoCs6, expressed the mesothelial markers *KRT19*, *TM4SF1*, and *EZR*, but to varying extents (Figures S7E and S7F). Furthermore, reference mapping revealed that MesoCs subclusters aligned with previously identified MesoC sub populations, such as hMes1 and hMes2 of the Emont et al. dataset (Figure S7G). Interestingly, MesoCs6 (fibronectin 1 [FN1]) was almost devoid of mesothelial markers (Figure S7H, Massier et al.[12]) but showed an enrichment of the APC marker genes *PDGFRA* and *FN1* (Figure 5F), in agreement with a gradual increase in stem cell markers along the epithelial to mesenchymal transition (EMT). Based on the expression of marker genes, MesoCs1 (keratin 19 [KRT19]), MesoCs3 (cluster of differentiation 55 [CD55]), and MesoCs4 (peroxisome proliferator-activated receptor gamma [PPARG]) represent cMesoCs (Figure S7I), and MesoCs2 (butyrylcholinesterase [BCHE]) and MesoCs5 (intelectin 1 [ITLN1]) correspond to meMesoC (Figure S7I).

Furthermore, we noted that only specific mesothelial subtypes were positively associated with metabolic health (Figures 5G and 5H). The fraction of MesoCs4 (PPARG) was significantly higher and MesoCs6 (FN1) trended to be higher in MUO (Figures 5G, 5H, and S7J). In contrast, the relative proportions of MesoCs2 (BCHE) and MesoCs5 (ITLN1) were increased in MHO (Figure 5G), which reached significance for MesoCs5 (ITLN1) upon demultiplexing of the dataset (Figure 5H). Additionally, many marker genes of MesoCs2 (BCHE) and MesoCs5 (ITLN1), such as *BCHE*, *CDON*, *DPP4*, *WT1*, and *ITLN1*, were upregulated in MesoCs in MHO and were also captured by MOFA-cell in visceral AT factor 1 driving the conditional separation (Figure S7K). Given that *ITLN1*, which encodes Omentin1, represents a well-described adipokine,[22] we aimed to investigate whether the health-dependent changes in the abundance of MesoCs5 (ITLN1) might have systemic effects. *ITLN1* was exclusively expressed by MesoCs within visceral AT (Figure 5I), and not present in subcutaneous AT (Figure S7L), recapitulating the previously described depot-specific expression pattern of *ITLN1*.[23] Furthermore, plasma Omentin1 levels were significantly higher in MHO compared with MUO (Figure 5J), establishing it as promising marker for visceral AT functionality.

Next, we investigated the marker gene expression of the mesothelial subpopulations in the bulk RNA-sequencing dataset. We identified that the expression of MesoCs1 (KRT19), MesoCs2 (BCHE), and MesoCs5 (ITLN1) markers was positively correlating with clinical parameters of metabolic health (Figures 5K and S8A). This association was not evident for marker genes of MesoCs3 (CD55), MesoCs4 (PPARG), and MesoCs6 (FN1) (Figure S8B). To further investigate the dependency of MesoCs subclusters and metabolic sequalae, we utilized an independent dataset of visceral AT of individuals at the time of bariatric surgery and 2-years post-surgery (n = 44) achieving at least 25% of BMI loss (clinical data summary in

Figure 5. Transitioning of mesothelial cells along the epithelial to mesenchymal state strongly correlates with metabolic health

(A and B) Feature plot showing expression of (A) *BCHE* and (B) *KRT19* in visceral AT.

(C) Violin plots showing estimated relative proportions of classical mesothelial cells (cMesoCs) and mesenchymal mesothelial cells (meMesoCs) from the bulk RNA-sequencing deconvolution of visceral AT of individuals with MHO (n = 31) and MUO (n = 43).

(D) RNA-scope staining showing BCHE-positive cells in visceral AT of a woman with MHO.

(E) UMAP of 5,310 nuclei representing visceral MesoCs of individuals split by MHO and MUO.

(F) Dot plot showing expression of markers genes used for annotating mesothelial sub populations in visceral AT.

(G) Bar plots showing relative proportions of visceral MesoCs subpopulations in MHO and MUO.

(H) Violin plots showing relative MesoCs subtype proportions of SNP-demultiplexed individuals with MHO and MUO in visceral AT.

(I) Feature plot showing expression of *ITLN1* in visceral AT.

(J) Plasma Ometin1 level distribution between individuals with MHO (n = 32) and MUO (n = 45).

(K) Spearman correlation plot showing positive and negative correlations between MesoCs1, MesoCs2, and MesoCs5 marker gene expression in the bulk RNA-sequencing data and indicated clinical parameters. Color scale represents Spearman correlation coefficient values. Significant correlations are indicated by asterisks. (*p < 0.05, **p < 0.01, ***p < 0.001).

(L) PCA of pseudobulk data from SNP-demultiplexed individuals showing cluster formation of visceral MesoCs between MHO and MUO, split by sex.

(M and N) Top significant (M) upregulated and (N) downregulated WikiPathways in visceral MesoCs of individuals with MUO vs. MHO.

Statistical significance was analyzed by two-tailed unpaired t test (C, H, and J), or Spearman correlation test (K). (Abbreviations: adipose tissue, AT; mesothelial cells, MesoCs; classical mesothelial cells, cMesoCs; and mesenchymal mesothelial cells, meMesoCs).

Please cite this article in press as: Reinisch et al., Unveiling adipose populations linked to metabolic health in obesity, Cell Metabolism (2024), https://doi.org/10.1016/j.cmet.2024.11.006

Table S5). Analysis of bulk RNA-sequencing data of this cohort revealed that several MesoCs1 (KRT19), MesoCs2 (BCHE), and MesoCs5 (ITLN1) markers were significantly increased post-bariatric surgery weight loss (Figure S8C), whereas markers for other MesoC subtypes remained unchanged (Figure S8D).

Furthermore, MesoCs showed conditional separation in pseudobulk analysis comparing MHO and MUO (Figure 5L), confirming that they undergo major transcriptional changes in dependence on health status. Upregulated genes of MesoCs in visceral AT of MUO were enriched for inflammatory pathways (Figure 5M), whereas the hedgehog signaling pathway and PDGFR signaling were increased in MesoCs under healthy conditions (Figure 5N). These data suggest that MesoCs might undergo a switch from a mesenchymal to an inflammatory phenotype under disease conditions, providing additional evidence for an improtant function of MesoCs in visceral AT remodeling.

DISCUSSION

AT plasticity is orchestrated by the abundance and interaction of various cell types in specialized niches, and a decrease in this cellular flexibility ignites tissue dysfunction.[10] Furthermore, each anatomical adipose depot displays a distinct pattern of cell composition, functionality, and disease propensity and uniquely responds to metabolically demanding conditions.[24] By using snRNA sequencing in combination with deconvolution of bulk RNA-sequencing datasets and unsupervised MOFA-cell, we generated a map representative of cellular maladaptions in obesity and identified cell types that are strongly associated with metabolic sequelae. Overall, dissecting AT at a single-nucleus resolution was superior to bulk transcriptomics in identifying AT-specific signatures that correlate with clinical parameters of the metabolic syndrome. Furthermore, these datasets admitted the identification of several visceral AT populations and transcriptional programs, which were strongly associated with the disease state.

Multiple mechanisms for the paradoxical retainment of metabolic health in obesity have been discussed, among them, low visceral fat mass and maintained AT function have been proposed as confounding factors.[2,4,25,26] Unhealthy AT distribution can be observed in multiple clinically manifested disease that are associated with metabolic abnormalities, e.g., lipodystrophy, lipodystrophy-like conditions, and Cushing's disease.[3] Genome-wide association study (GWAS) studies showed that metabolic-health-associated genes are enriched in adipocytes,[27] linking adipocyte dysfunction to disease. Furthermore, the overexpression of the adipokine adiponectin[28] or AT-derived mitochondrial protein mitoNEET[29] in genetically obese mice can mimic the phenotype of human MHO, providing additional evidence that AT function is a confounding factor for metabolic health. Whereas MHO should not be considered a condition that does not require treatment, as it might represent a transient phenotype,[2] it offers a unique opportunity to study the relationship between AT dysfunction and severity of metabolic disease in humans.

Adipocyte heterogeneity within a single depot is a recent concept that has been introduced by findings from single-nucleus studies.[30] Collectively, studies have shown that the proportion of lipogenic adipocyte subpopulations was negatively associated with BMI[11,13] and T2D,[11] aligning with enhanced *in vivo* insulin sensitivity of isolated lipogenic adipocytes[13] and increased lipogenesis in subcutaneous adipocytes of individuals with MHO.[31] Other adipocyte subpopulations (Adipo^{LEP} and hAd5) were positively associated with T2D,[11,12] suggesting that specific adipocyte subtypes have an inverse association with the metabolic health state. In our dataset, MUO was characterized by an overall lower number of adipocytes in both adipose depots, and subsequent adipocyte hypertrophy. On the subcluster level, we identified three common[10] and two depot-specific adipocyte populations in visceral and subcutaneous AT. The visceral-specific vAdipo4 (FGF14) corresponds to previously identified thermogenic adipocytes hAd6, reinforcing that human visceral AT may be prone to browning.[11] Whereas the amount of distinct visceral adipocyte subpopulations was unchanged, visceral adipocytes of MUO were characterized by a shift from a metabolic to a hypoxic phenotype. In subcutaneous AT, adipocytes represented the cell type, which was most strongly linked to metabolic health. We identified a distinct inflammatory subcutaneous subpopulation (sAdipo5 [NRCAM]), marked by *NRCAM*, which was significantly overrepresented in MUO. A similar NRCAM-positive adipocyte population has previously been associated with clinical conditions, as shown by a positive correlation between the marker gene for this population and LDL levels.[11]

In addition to the intrinsic development of the metabolic inflexibility in adipocytes, impairments in the adipogenic capacity is a hallmark of adipocyte dysfunction.[32] In line with previous single-nucleus studies showing that the abundance of distinct progenitor populations was strongly associated with metabolic health,[12] we found that CPAs1 (FMO2) were reduced in visceral AT of MUO compared with MHO. Strikingly, the abundance of several other visceral APCs subpopulations showed a strong sex dimorphism, and transcriptional differences in APCs were the greatest discriminant of men and women in visceral AT under MUO. We identified a visceral-specific ephrin type-A receptor 3 (EPHA3)-positive AAP population (Emont et al.[11] AAPs2 [ZNF804B]), which was strongly present in women with MUO, but almost undetectable in any other group. AAPs have been shown to suppress adipocyte formation through paracrine mechanisms,[33,34] which was in conjunction with the reduced expression of adipogenic pathways in visceral APCs and the lower relative abundance of CPAs2 (ICAM1), when we compared women with men with MUO. Furthermore, based on the high expression of cytokines in AAPs2 and positive relationship of AAPs2 with adaptive immune cells, we surmise that AAPs2 can either directly restrict adipogenesis by interaction with other APCs in their niche, or secondary to the recruitment of adaptive immune cells. Previously published data showed that APCs secrete *CCL5*, which triggered the infiltration of T cells into AT in the early stages of obesity.[35] Additionally, the expression of *CCL5* in visceral AT or isolated APCs of humans showed a positive relationship with BMI.[35] Furthermore, obese female mice showed improved metabolic health compared with obese males, with more regulatory T cells, fewer visceral AT macrophages and higher insulin sensitivity.[35] This aligns with our findings, where women with MUO had better metabolic profiles, more adaptive immune cells, and lower macrophage counts in visceral AT

Please cite this article in press as: Reinisch et al., Unveiling adipose populations linked to metabolic health in obesity, Cell Metabolism (2024), https://doi.org/10.1016/j.cmet.2024.11.006

than men. Together, our results suggests that sex has a strong impact on the metabolic-health-dependent changes in APCs, most prominently shown by the selective presence of one visceral-specific, adipogenesis-regulatory cell type in women with MUO. The potential interplay between APCs, adaptive immune cells, and macrophages may partially explain the observed sexual dimorphism in AT function and the progression of metabolic disorders.

Besides being the protective barrier of visceral AT, MesoCs can secrete chemokines, contributing to development of AT inflammation.[21,36] Correlating cell type abundance and marker gene expression with clinical parameters, and MOFA-cell analysis revealed distinct mesothelial subtypes (meMesoCs) as key factors linking AT composition with metabolic health. Furthermore, data from our study points to the direction that visceral AT MesoCs can adopt different phenotypes along the epithelial to mesenchymal landscape, which is strongly influenced by systemic health conditions. Early reports on potential adipogenic-properties of these cells have been controversial, with data of lineage-tracing models proposing that MesoCs are a source of adipocytes,[37] which was questioned by later studies showing the markers used in these studies were not specific.[38] Only recently, there is a regained interest in MesoCs as potential contributors to the pool of adipocyte precursors, with a study showing that distinct human mesothelial subpopulations were enriched in markers for EMT.[14] During EMT, epithelial cells lose their apical-basal polarity and cell-cell adhesive properties, adopting a migratory, mesenchymal cell phenotype.[39] This cell-identity switch has been well described in the context of cancer development, embryogenesis, and wound healing,[39] but there is so far no direct evidence of MesoCs undergoing EMT in AT. Although a precise mechanism responsible for MesoC plasticity cannot be determined in our study, we surmise that under healthy conditions, the environmental-niche and/or cell-intrinsic factors may promote EMT in MesoCs. This might guarantee a steady supply of newly differentiated adipocytes from the tissue surroundings and prevent AT dysfunction.

Personalized treatment options represent the standard of care for many metabolic diseases, such as cancer,[40] but are still not applied in obesity treatment. Furthermore, although the BMI is a simple and clinically easily applicable surrogate for adiposity, studies showed that obesity defined by this metric is heterogeneous and that individuals with similar BMI or body weight have remarkable differences in health risk.[41] In this study, we used MHO as a human model to screen cellular confounders of the metabolic heterogeneity among obese. Thereby, our study extends on previous datasets by clearly stratifying individuals based on the degree of metabolic disease. We identified several visceral-specific cell populations that were associated with the metabolic syndrome, like MesoCs, adipocytes and APCs. In line with the enlarged visceral depot volume in MUO, our dataset reinforces that AT distribution and function is intimately linked to human health. Furthermore, adipocyte-specific transcriptional analysis revealed that both visceral and subcutaneous adipocytes distinguish between MHO and MUO.

Together, we generated the first dataset for single-cell transcriptomics of visceral and subcutaneous AT under clearly defined metabolic health conditions. This resource provides a unique opportunity to study AT subpopulations that are involved in tissue dysfunction and investigate disease-related pathways and can be used to find novel visceral-specific biomarkers to monitor the transition from MHO to MUO and vice versa.

Limitations of the study

The snRNA-sequencing data of this study was only generated on pooled samples and demultiplexed with bioinformatic approaches based on called SNPs. This approach does not allow us to perform any association tests with clinical data at the cell-type level due to missing genetics information at the individual level. Furthermore, the cell-type abundance is an estimate and does not reflect true proportions in the AT depot. Future studies should focus on the physiological function of the newly defined cell types (such as AAP2s [ZNF804B] and meMesoCs) and investigate if they are causally involved in driving metabolic disease. Additionally, this study did not stratify individuals according to age, which is a strong confounder for metabolic disease development. Another limitation is that we did not have the chance to sample the biopsies longitudinally, which prevented us from predicting if a transition from an MHO to MUO state or vice versa could indeed be associated with compositional differences of the discussed cell populations. Furthermore, we cannot rule out that a bias toward distinct nuclei (depending on size or abundance) for snRNA-sequencing experiments exists. Lastly, although the whole cohort compromised a relatively large number of individuals, the sample size became quite small after stratifying by sex and might be underpowered.

RESOURCE AVAILABILITY

Lead contact

Requests for further information and resources should be directed to the lead contact, Prof. Christian Wolfrum (christian-wolfrum@ethz.ch).

Materials availability

This study did not generate new unique reagents.

Data and code availability

- Bulk RNA and snRNA-sequencing data reported in this study cannot be deposited in a public repository due to restrictions by patient consent, but they are available from the lead contact upon request.
- This paper does not report original code.
- Analysis code and web application links to explore the datasets are available on GitHub (https://github.com/WolfrumLab/MHUO/).
- Original data for generating all graphs in the manuscripts are provided in Data S1 (unprocessed data underlying the display items in the manuscript, related to Figures 1, 2, 3, 4, 5, and S1–S8).
- Any additional information required to reanalyze the data reported in this paper is available from the lead contact upon request.

ACKNOWLEDGMENTS

We are grateful to the study participants. We thank M.R. Schön, D. Gärtner, T. Lohmann, and M. Dressler for contributing adipose tissue biopsies. We appreciate the feedback from B. Noyvert and A. King on the quality control of bulk transcriptomics data. We also thank Functional Genomics Center Zurich for providing the computational infrastructure for all bioinformatics analyses. This work was supported by the German Research Foundation (Deutsche Forschungsgemeinschaft CRC 1052, project number 209933838, subproject B1 to M.B.) and Swiss National Science Foundation (SNSF 185011 and SNSF

215605 to C.W.). I.R. was supported by the Austrian Science Fund FWF (Schroedinger stipend J4760).

AUTHOR CONTRIBUTIONS

I.R. and A.G. contributed equally. I.R., A.G., M.B., and C.W. conceptualized the study. A.D., A.H., and M.B. provided adipose tissue samples and clinical data. W.S. and H.D. made bulk RNA-sequencing libraries. I.R. made single-nuclei RNA-sequencing libraries and performed histological assays. A.G., I.R., and F.N. analyzed the data. A.G., P.L., and F.N. developed the interactive web applications. M.B. and C.W. supervised the study. I.R., A.G., and C.W. wrote the manuscript. All authors contributed to editing and reviewing the manuscript.

DECLARATION OF INTERESTS

M.B. received honoraria as a consultant and speaker from Amgen, AstraZeneca., Bayer, Boehringer-Ingelheim, Lilly, Novo Nordisk, and Sanofi.

STAR★METHODS

Detailed methods are provided in the online version of this paper and include the following:

- KEY RESOURCES TABLE
- EXPERIMENTAL MODEL AND STUDY PARTICIPANT DETAILS
  - Study design of clinical cohorts
- METHOD DETAILS
  - Bulk RNA sequencing
  - snRNA-sequencing
  - Correlation analysis with clinical parameters
  - RNA-scope based stainings
  - Statistical analysis

SUPPLEMENTAL INFORMATION

Supplemental information can be found online at https://doi.org/10.1016/j.cmet.2024.11.006.

Received: February 9, 2024
Revised: August 6, 2024
Accepted: November 10, 2024
Published: December 17, 2024

REFERENCES

1. Blüher, M. (2019). Obesity: global epidemiology and pathogenesis. Nat. Rev. Endocrinol. *15*, 288–298. https://doi.org/10.1038/s41574-019-0176-8.
2. Blüher, M. (2020). Metabolically healthy obesity. Endocr. Rev. *41*, 405–420. https://doi.org/10.1210/endrev/bnaa004.
3. Stefan, N. (2020). Causes, consequences, and treatment of metabolically unhealthy fat distribution. Lancet Diabetes Endocrinol. *8*, 616–627. https://doi.org/10.1016/S2213-8587(20)30110-8.
4. Klöting, N., Fasshauer, M., Dietrich, A., Kovacs, P., Schön, M.R., Kern, M., Stumvoll, M., and Blüher, M. (2010). Insulin-sensitive obesity. Am. J. Physiol. Endocrinol. Metab. *299*, E506–E515. https://doi.org/10.1152/ajpendo.00586.2009.
5. Karpe, F., and Pinnick, K.E. (2015). Biology of upper-body and lower-body adipose tissue—link to whole-body phenotypes. Nat. Rev. Endocrinol. *11*, 90–100. https://doi.org/10.1038/nrendo.2014.185.
6. Lee, M.-J., Wu, Y., and Fried, S.K. (2013). Adipose tissue heterogeneity: implication of depot differences in adipose tissue for obesity complications. Mol. Aspects Med. *34*, 1–11. https://doi.org/10.1016/j.mam.2012.10.001.
7. Di Angelantonio, E., Di Angelantonio, E., Bhupathiraju, S.N., Wormser, D., Gao, P., Kaptoge, S., Berrington de Gonzalez, A., Cairns, B.J., Huxley, R., Jackson, C.L., et al. (2016). Body-mass index and all-cause mortality: individual-participant-data meta-analysis of 239 prospective studies in four continents. Lancet *388*, 776–786. https://doi.org/10.1016/S0140-6736(16)30175-1.
8. Ghaben, A.L., and Scherer, P.E. (2019). Adipogenesis and metabolic health. Nat. Rev. Mol. Cell Biol. *20*, 242–258. https://doi.org/10.1038/s41580-018-0093-z.
9. Sakers, A., De Siqueira, M.K., Seale, P., and Villanueva, C.J. (2022). Adipose-tissue plasticity in health and disease. Cell *185*, 419–446. https://doi.org/10.1016/j.cell.2021.12.016.
10. Maniyadath, B., Zhang, Q., Gupta, R.K., and Mandrup, S. (2023). Adipose tissue at single-cell resolution. Cell Metab. *35*, 386–413. https://doi.org/10.1016/j.cmet.2023.02.002.
11. Emont, M.P., Jacobs, C., Essene, A.L., Pant, D., Tenen, D., Colleluori, G., Di Vincenzo, A., Jørgensen, A.M., Dashti, H., Stefek, A., et al. (2022). A single-cell atlas of human and mouse white adipose tissue. Nature *603*, 926–933. https://doi.org/10.1038/s41586-022-04518-2.
12. Massier, L., Jalkanen, J., Elmastas, M., Zhong, J., Wang, T., Nono Nankam, P.A., Frendo-Cumbo, S., Bäckdahl, J., Subramanian, N., Sekine, T., et al. (2023). An integrated single cell and spatial transcriptomic map of human white adipose tissue. Nat. Commun. *14*, 1438. https://doi.org/10.1038/s41467-023-36983-2.
13. Bäckdahl, J., Franzén, L., Massier, L., Li, Q., Jalkanen, J., Gao, H., Andersson, A., Bhalla, N., Thorell, A., Rydén, M., et al. (2021). Spatial mapping reveals human adipocyte subpopulations with distinct sensitivities to insulin. Cell Metab. *33*, 1869–1882.e6. https://doi.org/10.1016/j.cmet.2021.07.018.
14. Ferrero, R., Rainer, P.Y., Rumpler, M., Russeil, J., Zachara, M., Pezoldt, J., van Mierlo, G., Gardeux, V., Saelens, W., Alpern, D., et al. (2024). A human omentum-specific mesothelial-like stromal population inhibits adipogenesis through IGFBP2 secretion. Cell Metab. *36*, 1566–1585.e9. https://doi.org/10.1016/j.cmet.2024.04.017.
15. Ramirez Flores, R.O.R., Lanzer, J.D., Dimitrov, D., Velten, B., and Saez-Rodriguez, J. (2023). Multicellular factor analysis of single-cell data for a tissue-centric understanding of disease. eLife *12*, 1–27. https://doi.org/10.7554/eLife.93161.
16. Palmer, B.F., and Clegg, D.J. (2015). The sexual dimorphism of obesity. Mol. Cell. Endocrinol. *402*, 113–119. https://doi.org/10.1016/j.mce.2014.11.029.
17. Hagberg, C.E., and Spalding, K.L. (2024). White adipocyte dysfunction and obesity-associated pathologies in humans. Nat. Rev. Mol. Cell Biol. *25*, 270–289. https://doi.org/10.1038/s41580-023-00680-1.
18. Sárvári, A.K., Van Hauwaert, E.L., Markussen, L.K., Gammelmark, E., Marcher, A.-B., Ebbesen, M.F., Nielsen, R., Brewer, J.R., Madsen, J.G.S., and Mandrup, S. (2021). Plasticity of Epididymal Adipose Tissue in Response to Diet-Induced Obesity at Single-Nucleus Resolution. Cell Metab. *33*, 437–453.e5. https://doi.org/10.1016/j.cmet.2020.12.004.
19. Blüher, M. (2009). Adipose Tissue Dysfunction in Obesity. Exp. Clin. Endocrinol. Diabetes *117*, 241–250. https://doi.org/10.1055/s-0029-1192044.
20. Ferrero, R., Rainer, P., and Deplancke, B. (2020). Toward a Consensus View of Mammalian Adipocyte Stem and Progenitor Cell Heterogeneity. Trends Cell Biol. *30*, 937–950. https://doi.org/10.1016/j.tcb.2020.09.007.
21. Gupta, O.T., and Gupta, R.K. (2015). Visceral Adipose Tissue Mesothelial Cells: Living on the Edge or Just Taking Up Space? Trends Endocrinol. Metab. *26*, 515–523. https://doi.org/10.1016/j.tem.2015.07.003.
22. Tan, B.K., Adya, R., Farhatullah, S., Lewandowski, K.C., O'Hare, P., Lehnert, H., and Randeva, H.S. (2008). Omentin-1, a novel adipokine, is decreased in overweight insulin-resistant women with polycystic ovary syndrome: ex vivo and in vivo regulation of omentin-1 by insulin and glucose. Diabetes *57*, 801–808. https://doi.org/10.2337/db07-0990.
23. Fain, J.N., Sacks, H.S., Buehrer, B., Bahouth, S.W., Garrett, E., Wolf, R.Y., Carter, R.A., Tichansky, D.S., and Madan, A.K. (2008). Identification of omentin mRNA in human epicardial adipose tissue: comparison to omentin in subcutaneous, internal mammary artery periadventitial and visceral

abdominal depots. Int. J. Obes. (Lond) *32*, 810–815. https://doi.org/10.1038/sj.ijo.0803790.

24. Zwick, R.K., Guerrero-Juarez, C.F., Horsley, V., and Plikus, M.V. (2018). Anatomical, Physiological, and Functional Diversity of Adipose Tissue. Cell Metab. *27*, 68–83. https://doi.org/10.1016/j.cmet.2017.12.002.
25. Harman-Boehm, I., Blüher, M., Redel, H., Sion-Vardy, N., Ovadia, S., Avinoach, E., Shai, I., Klöting, N., Stumvoll, M., Bashan, N., and Rudich, A. (2007). Macrophage Infiltration into Omental Versus Subcutaneous Fat across Different Populations: Effect of Regional Adiposity and the Comorbidities of Obesity. J. Clin. Endocrinol. Metab. *92*, 2240–2247. https://doi.org/10.1210/jc.2006-1811.
26. Cancello, R., Henegar, C., Viguerie, N., Taleb, S., Poitou, C., Rouault, C., Coupaye, M., Pelloux, V., Hugol, D., Bouillot, J.-L., et al. (2005). Reduction of Macrophage Infiltration and Chemoattractant Gene Expression Changes in White Adipose Tissue of Morbidly Obese Subjects After Surgery-Induced Weight Loss. Diabetes *54*, 2277–2286. https://doi.org/10.2337/diabetes.54.8.2277.
27. Huang, L.O., Rauch, A., Mazzaferro, E., Preuss, M., Carobbio, S., Bayrak, C.S., Chami, N., Wang, Z., Schick, U.M., Yang, N., et al. (2021). Genome-wide discovery of genetic loci that uncouple excess adiposity from its comorbidities. Nat. Metab. *3*, 228–243. https://doi.org/10.1038/s42255-021-00346-2.
28. Kim, J.-Y., van de Wall, E., Laplante, M., Azzara, A., Trujillo, M.E., Hofmann, S.M., Schraw, T., Durand, J.L., Li, H., Li, G., et al. (2007). Obesity-associated improvements in metabolic profile through expansion of adipose tissue. J. Clin. Invest. *117*, 2621–2637. https://doi.org/10.1172/JCI31021.
29. Kusminski, C.M., Holland, W.L., Sun, K., Park, J., Spurgin, S.B., Lin, Y., Askew, G.R., Simcox, J.A., McClain, D.A., Li, C., and Scherer, P.E. (2012). MitoNEET-driven alterations in adipocyte mitochondrial activity reveal a crucial adaptive process that preserves insulin sensitivity in obesity. Nat. Med. *18*, 1539–1549. https://doi.org/10.1038/nm.2899.
30. Yang Loureiro, Z., Solivan-Rivera, J., and Corvera, S. (2022). Adipocyte Heterogeneity Underlying Adipose Tissue Functions. Endocrinology *163*, 1–7. https://doi.org/10.1210/endocr/bqab138.
31. Petersen, M.C., Smith, G.I., Palacios, H.H., Farabi, S.S., Yoshino, M., Yoshino, J., Cho, K., Davila-Roman, V.G., Shankaran, M., Barve, R.A., et al. (2024). Cardiometabolic characteristics of people with metabolically healthy and unhealthy obesity. Cell Metab. *36*, 745–761.e5. https://doi.org/10.1016/j.cmet.2024.03.002.
32. Meissburger, B., Ukropec, J., Roeder, E., Beaton, N., Geiger, M., Teupser, D., Civan, B., Langhans, W., Nawroth, P.P., Gasperikova, D., et al. (2011). Adipogenesis and insulin sensitivity in obesity are regulated by retinoid-related orphan receptor gamma. EMBO Mol. Med. *3*, 637–651. https://doi.org/10.1002/emmm.201100172.
33. Merrick, D., Sakers, A., Irgebay, Z., Okada, C., Calvert, C., Morley, M.P., Percec, I., and Seale, P. (2019). Identification of a mesenchymal progenitor cell hierarchy in adipose tissue. Science *364*, eaav2501. https://doi.org/10.1126/science.aav2501.
34. Schwalie, P.C., Dong, H., Zachara, M., Russeil, J., Alpern, D., Akchiche, N., Caprara, C., Sun, W., Schlaudraff, K.-U.U., Soldati, G., et al. (2018). A stromal cell population that inhibits adipogenesis in mammalian fat depots. Nature *559*, 103–108. https://doi.org/10.1038/s41586-018-0226-8.
35. Liao, X., Zeng, Q., Xie, L., Zhang, H., Hu, W., Xiao, L., Zhou, H., Wang, F., Xie, W., Song, J., et al. (2024). Adipose stem cells control obesity-induced T cell infiltration into adipose tissue. Cell Rep. *43*, 113963. https://doi.org/10.1016/j.celrep.2024.113963.
36. Darimont, C., Avanti, O., Blancher, F., Wagniere, S., Mansourian, R., Zbinden, I., Leone-Vautravers, P., Fuerholz, A., Giusti, V., and Macé, K. (2008). Contribution of mesothelial cells in the expression of inflammatory-related factors in omental adipose tissue of obese subjects. Int. J. Obes. (Lond) *32*, 112–120. https://doi.org/10.1038/sj.ijo.0803688.
37. Chau, Y.-Y., Bandiera, R., Serrels, A., Martínez-Estrada, O.M., Qing, W., Lee, M., Slight, J., Thornburn, A., Berry, R., McHaffie, S., et al. (2014). Visceral and subcutaneous fat have different origins and evidence supports a mesothelial source. Nat. Cell Biol. *16*, 367–375. https://doi.org/10.1038/ncb2922.
38. Westcott, G.P., Emont, M.P., Li, J., Jacobs, C., Tsai, L., and Rosen, E.D. (2021). Mesothelial cells are not a source of adipocytes in mice. Cell Rep. *36*, 109388. https://doi.org/10.1016/j.celrep.2021.109388.
39. Haerinck, J., Goossens, S., and Berx, G. (2023). The epithelial–mesenchymal plasticity landscape: principles of design and mechanisms of regulation. Nat. Rev. Genet. *24*, 590–609. https://doi.org/10.1038/s41576-023-00601-0.
40. Bhinder, B., Gilvary, C., Madhukar, N.S., and Elemento, O. (2021). Artificial Intelligence in Cancer Research and Precision Medicine. Cancer Discov. *11*, 900–915. https://doi.org/10.1158/2159-8290.CD-21-0090.
41. Neeland, I.J., Ross, R., Després, J.-P., Matsuzawa, Y., Yamashita, S., Shai, I., Seidell, J., Magni, P., Santos, R.D., Arsenault, B., et al. (2019). Visceral and ectopic fat, atherosclerosis, and cardiometabolic disease: a position statement. Lancet Diabetes Endocrinol. *7*, 715–725. https://doi.org/10.1016/S2213-8587(19)30084-1.
42. Chen, S., Zhou, Y., Chen, Y., and Gu, J. (2018). fastp: an ultra-fast all-in-one FASTQ preprocessor. Bioinformatics *34*, i884–i890. https://doi.org/10.1093/bioinformatics/bty560.
43. Bray, N.L., Pimentel, H., Melsted, P., and Pachter, L. (2016). Near-optimal probabilistic RNA-seq quantification. Nat. Biotechnol. *34*, 525–527. https://doi.org/10.1038/nbt.3519.
44. Love, M.I., Huber, W., and Anders, S. (2014). Moderated estimation of fold change and dispersion for RNA-seq data with DESeq2. Genome Biol. *15*, 550. https://doi.org/10.1186/s13059-014-0550-8.
45. Ritchie, M.E., Phipson, B., Wu, D., Hu, Y., Law, C.W., Shi, W., and Smyth, G.K. (2015). limma powers differential expression analyses for RNA-sequencing and microarray studies. Nucleic Acids Res. *43*, e47. https://doi.org/10.1093/nar/gkv007.
46. Zheng, G.X.Y., Terry, J.M., Belgrader, P., Ryvkin, P., Bent, Z.W., Wilson, R., Ziraldo, S.B., Wheeler, T.D., McDermott, G.P., Zhu, J., et al. (2017). Massively parallel digital transcriptional profiling of single cells. Nat. Commun. *8*, 14049. https://doi.org/10.1038/ncomms14049.
47. Butler, A., Hoffman, P., Smibert, P., Papalexi, E., and Satija, R. (2018). Integrating single-cell transcriptomic data across different conditions, technologies, and species. Nat. Biotechnol. *36*, 411–420. https://doi.org/10.1038/nbt.4096.
48. Hao, Y., Hao, S., Andersen-Nissen, E., Mauck, W.M., Zheng, S., Butler, A., Lee, M.J., Wilk, A.J., Darby, C., Zager, M., et al. (2021). Integrated analysis of multimodal single-cell data. Cell *184*, 3573–3587.e29. https://doi.org/10.1016/j.cell.2021.04.048.
49. Germain, P.-L., Lun, A., Garcia Meixide, C., Macnair, W., and Robinson, M.D. (2021). Doublet identification in single-cell sequencing data using scDblFinder. F1000Res *10*, 979. https://doi.org/10.12688/f1000research.73600.2.
50. Blanco-Carmona, E. (2022). Generating publication ready visualizations for Single Cell transcriptomics using SCpubr. Preprint at bioRxiv.
51. Jin, S., Guerrero-Juarez, C.F., Zhang, L., Chang, I., Ramos, R., Kuan, C.-H., Myung, P., Plikus, M.V., and Nie, Q. (2021). Inference and analysis of cell-cell communication using CellChat. Nat. Commun. *12*, 1088. https://doi.org/10.1038/s41467-021-21246-9.
52. Jew, B., Alvarez, M., Rahmani, E., Miao, Z., Ko, A., Garske, K.M., Sul, J.H., Pietiläinen, K.H., Pajukanta, P., and Halperin, E. (2020). Accurate estimation of cell composition in bulk expression through robust integration of single-cell information. Nat. Commun. *11*, 1971. https://doi.org/10.1038/s41467-020-15816-6.
53. Huang, X., and Huang, Y. (2021). Cellsnp-lite: an efficient tool for genotyping single cells. Bioinformatics *37*, 4569–4571. https://doi.org/10.1093/bioinformatics/btab358.
54. Huang, Y., McCarthy, D.J., and Stegle, O. (2019). Vireo: Bayesian demultiplexing of pooled single-cell RNA-seq data without genotype reference. Genome Biol. *20*, 273. https://doi.org/10.1186/s13059-019-1865-2.

55. Robinson, M.D., McCarthy, D.J., and Smyth, G.K. (2010). edgeR: a Bioconductor package for differential expression analysis of digital gene expression data. Bioinformatics *26*, 139–140. https://doi.org/10.1093/bioinformatics/btp616.

56. Argelaguet, R., Arnol, D., Bredikhin, D., Deloro, Y., Velten, B., Marioni, J.C., and Stegle, O. (2020). MOFA+: A statistical framework for comprehensive integration of multi-modal single-cell data. Genome Biol. *21*, 111. https://doi.org/10.1186/s13059-020-02015-1.

57. Argelaguet, R., Velten, B., Arnol, D., Dietrich, S., Zenz, T., Marioni, J.C., Buettner, F., Huber, W., and Stegle, O. (2018). Multi-Omics Factor Analysis—a framework for unsupervised integration of multi-omics data sets. Mol. Syst. Biol. *14*, e8124. https://doi.org/10.15252/msb.20178124.

58. Langhardt, J., Flehmig, G., Klöting, N., Lehmann, S., Ebert, T., Kern, M., Schön, M.R., Gärtner, D., Lohmann, T., Dressler, M., et al. (2018). Effects of Weight Loss on Glutathione Peroxidase 3 Serum Concentrations and Adipose Tissue Expression in Human Obesity. Obes. Facts *11*, 475–490. https://doi.org/10.1159/000494295.

59. Hirsch, J., and Gallian, E. (1968). Methods for the determination of adipose cell size in man and animals. J. Lipid Res. *9*, 110–119. https://doi.org/10.1016/s0022-2275(20)43151-7.

60. Muir, L.A., Baker, N.A., Washabaugh, A.R., Neeley, C.K., Flesher, C.G., DelProposto, J.B., Geletka, L.M., Ghaferi, A.A., Finks, J.F., Singer, K., et al. (2017). Adipocyte hypertrophy-hyperplasia balance contributes to weight loss after bariatric surgery. Adipocyte *6*, 134–140. https://doi.org/10.1080/21623945.2017.1287639.

61. Mulhem, A., Moulla, Y., Klöting, N., Ebert, T., Tönjes, A., Fasshauer, M., Dietrich, A., Schön, M.R., Stumvoll, M., Richter, V., et al. (2021). Circulating cell adhesion molecules in metabolically healthy obesity. Int. J. Obes. (Lond) *45*, 331–336. https://doi.org/10.1038/s41366-020-00667-4.

62. Picelli, S., Faridani, O.R., Björklund, A.K., Winberg, G., Sagasser, S., and Sandberg, R. (2014). Full-length RNA-seq from single cells using Smart-seq2. Nat. Protoc. *9*, 171–181. https://doi.org/10.1038/nprot.2014.006.

63. Song, Y., Milon, B., Ott, S., Zhao, X., Sadzewicz, L., Shetty, A., Boger, E.T., Tallon, L.J., Morell, R.J., Mahurkar, A., et al. (2018). A comparative analysis of library prep approaches for sequencing low input translatome samples. BMC Genomics *19*, 696. https://doi.org/10.1186/s12864-018-5066-2.

64. Kuleshov, M.V., Jones, M.R., Rouillard, A.D., Fernandez, N.F., Duan, Q., Wang, Z., Koplev, S., Jenkins, S.L., Jagodnik, K.M., Lachmann, A., et al. (2016). Enrichr: a comprehensive gene set enrichment analysis web server 2016 update. Nucleic Acids Res. *44*, W90–W97. https://doi.org/10.1093/nar/gkw377.

Please cite this article in press as: Reinisch et al., Unveiling adipose populations linked to metabolic health in obesity, Cell Metabolism (2024), https://doi.org/10.1016/j.cmet.2024.11.006

CellPress
OPEN ACCESS

STAR★METHODS

KEY RESOURCES TABLE

REAGENT or RESOURCE	SOURCE	IDENTIFIER
Antibodies		
TSA OPAL 570	Akoya Biosciences	FP1488001KT
TSA Opal 650	Akoya Biosciences	FP1496001KT
Biological samples		
Human subcutaneous and visceral adipose tissue	Leipzig Obesity BioBank	https://www.helmholtz-munich.de/en/hi-mag/cohort/leipzig-obesity-bio-bank-lobb
Chemicals, peptides, and recombinant proteins		
Prolong Gold Antifade Mountant	Thermo Fisher	P36934
RNAse Inhibitor	Takara	2313A
Critical commercial assays		
RNAscope Multiplex Fluorescent V2 assay	Bio-techne	Cat. No. 323110
Chromium Single Cell V3.4	10X Genomics	PN-1000691, PN-1000690, PN-1000215
Illumina DNA Prep	Illumina	20060060
Deposited data		
Bulk RNA-seq data from subcutaneous and visceral adipose tissue	This paper	Available upon request from M.B. and C.W.
snRNA-seq data from subcutaneous and visceral adipose tissue	This paper	Available upon request from C.W.
Oligonucleotides		
Hs 3plex positive control	Bio-techne	PN 320861
3Plex negative control	Bio-techne	PN 320871
Hs-BCHE-C1	Bio-techne	502331-C2
Hs-ZNF804B-C1	Bio-techne	526131
Software and algorithms		
fastp	Chen et al.[42]	https://github.com/OpenGene/fastp
Kallisto	Bray et al.[43]	https://github.com/pachterlab/kallisto
DESeq2	Love et al.[44]	https://bioconductor.org/packages/release/bioc/html/DESeq2.html
Limma	Ritchie et al.[45]	https://www.bioconductor.org/packages/release/bioc/html/limma.html
CellRanger	Zheng et al.[46]	https://www.10xgenomics.com/support/software/cell-ranger/
Seurat	Butlet et al.[47] Hao et al.[48]	https://satijalab.org/seurat/
scDblFinder	Germain et al.[49]	https://github.com/plger/scDblFinder
SCpubr	Blanco-Carmona et al.[50]	https://github.com/enblacar/SCpubr
CellChat	Jin et al.[51]	https://github.com/sqjin/CellChat
BisqueRNA	Jew et al.[52]	https://github.com/cran/BisqueRNA
Cellsnp-lite	Huang et al.[53]	https://github.com/single-cell-genetics/cellsnp-lite
vireo	Huang et al.[54]	https://github.com/single-cell-genetics/vireo
edgeR	Robinson et al.[55]	https://bioconductor.org/packages/release/bioc/html/edgeR.html
MOFAcellulaR	Flores et al.[15]	https://github.com/saezlab/MOFAcellulaR
MOFA2	Argelaguet et al.[56,57]	https://biofam.github.io/MOFA2/
R version 4.4	R Foundation	https://www.r-project.org/
RStudio	Posit	https://posit.co/products/open-source/rstudio/

(*Continued on next page*)

Please cite this article in press as: Reinisch et al., Unveiling adipose populations linked to metabolic health in obesity, Cell Metabolism (2024), https://doi.org/10.1016/j.cmet.2024.11.006

Continued

REAGENT or RESOURCE	SOURCE	IDENTIFIER
GraphPad Prism version 10	GraphPad	https://www.graphpad.com/
Affinity	N/A	N/A
Other		
Resource website for the MHUO publication	This paper	https://github.com/WolfrumLab/MHUO/

EXPERIMENTAL MODEL AND STUDY PARTICIPANT DETAILS

Study design of clinical cohorts

Leipzig Obesity BioBank (https://www.helmholtz-munich.de/en/hi-mag/cohort/leipzig-obesity-bio-bank-lobb) is a comprehensive collection of human body fluids, AT samples and related clinical parameters, designed to enhance our understanding of obesity and its associated disorders across three different cohorts. Samples of omental visceral and abdominal subcutaneous AT were collected during elective laparoscopic abdominal surgery as previously described[58] and immediately frozen in liquid nitrogen and stored at -80°C. Measurements of body composition and metabolic parameters were performed as previously described.[4] In short, all patients had been examined in supine position in a single 1.5-T MRI system (Achieva XR, Philips Healthcare, Best, Netherlands) using the integrated whole-body coil for signal reception. The essential image series for fat quantification was a simple dual-echo gradient-echo pulse sequence with echo times matching opposed-phase and in-phase conditions using the following parameters: 50 transverse slices (two stacks covering the abdominopelvic region between diaphragm and pubic symphysis), slice thickness 10 mm thick, interslice gap 0.5 mm, echo times 2.3 ms and 4.6 ms, repetition time 76 ms, flip angle 70°, field of view 530 mm × 530 mm, acquisition matrix 216 × 177 and reconstruction matrix 480 × 480. Adipocyte cell size, as well as macrophage count and diameter, were analyzed using supervised automated analysis with CellSens software. The obtained mean adipocyte diameter ± standard error was computed in adipocyte volume using the Hirsh and Gallian formula.[59] Adipocyte volume was calculated as described previously.[60] Adipose tissue samples were collected in 37°C PBS buffer, and adipocytes were isolated by collagenase (1 mg/ml) digestion. For the determination of glucose transport, isolated adipocytes from the different fat depots were stimulated with 100 nM insulin for 30 min and then incubated for 30 min with 3 μM [U-14C] glucose. Immediately after incubation, adipocytes were fixed with osmic acid and incubated for 48 h at 37°C, and radioactivity was quantified after the cells had been decolorized. Glucose transport data were normalized for cell number. To determine adipocyte number and cell size distribution, 200μl aliquots of adipocytes were fixed with osmic acid, incubated for 48 h at 37°C, and counted in a Coulter counter (Multisizer III; Beckman Coulter, Krefeld, Germany).

The study was performed in agreement with the Declaration of Helsinki and approved by the Ethics Committee of the University of Leipzig (approval numbers 159-12-21052012, 017-12-23012012). Samples were only collected from adult male and female individuals who have provided written informed consent. Sample exclusion criteria included chronic substance or alcohol abuse, smoking within the last year leading up to surgery, terminal malignant disorders, uncontrolled thyroid disorders and Cushing's disease.

The MHO/MUO cohort included 32 insulin-sensitive individuals (IS; 71.8% female; age: 38.75 ± 10.98 years; BMI: 46 ± 6.82 kg/m^2; FPG: 5.22 ± 0.19 mmol/l; FPI: 28.74 ± 14.17 pmol/l) and 45 insulin-resistant individuals (IR; 71.1% female; age: 47.09 ± 7.49 years; BMI: 46.89 ± 8.12 kg/m^2; FPG: 5.67 ± 0.34 mmol/l; FPI: 107.96 ± 30.32 pmol/l) with obesity (Table S1), of whom we performed snRNA sequencing on pooled AT samples of 41 visceral and 36 subcutaneous depots (Tables S2 and S3). The study participants with obesity were stratified into metabolically healthy and unhealthy groups according to previously published parameters.[4,61]

From the cross-sectional study cohort, only metabolically healthy non-obese (MHNO) male individuals were considered who had undergone surgery at the Leipzig University Hospital. Visceral AT samples were collected from six MHNO individuals (age: 58.32 ± 18.02 years; BMI: 27.99 ± 5.35 kg/m^2; FPG: 5.05 ± 0.66 mmol/l; FPI: 14.58 ± 12.01 pmol/l; HOMA-IR: 0.45 ± 0.34) and subcutaneous AT samples were collected from four MHNO individuals (age: 68.25 ± 8.51 years; BMI: 26.44 ± 2.16 kg/m^2; FPG: 5.72 ± 0.48 mmol/l; FPI: 9.47 ± 7.97 pmol/l; HOMA-IR: 0.35 ± 0.29) for performing pooled snRNA sequencing (Table S4).

From the bariatric surgery cohort, only individuals with a BMI loss of more than 25% were considered for bulk RNA-sequencing. Visceral AT samples were collected from 44 individuals (73% female; age before surgery: 44.93 ± 9.56 years; BMI before surgery: 55.57 ± 10.4 kg/m^2; weight before surgery: 160.9 ± 29.63 kg) undergoing two-step bariatric surgery, with sleeve gastrectomy as the first step (t0) and Roux-en-Y gastric bypass as the second step (t1).[58] After both surgeries, on average, individuals lost 33.32 ± 6.3 kg/m^2 of BMI and 54.51 ± 16.13 kg of weight (Table S5). All individuals received personalized dietary recommendations during their regular visits to the obesity management center.

METHOD DETAILS

Bulk RNA sequencing

Library preparation and sequencing

rRNA-depleted RNA-sequencing data were prepared on the basis of the SMARTseq protocol.[62,63] Briefly, isolated RNA was treated with DNaseI and reverse transcribed using an oligo(dT) and a template switch oligo. cDNA was amplified using ISPCR primers and

Please cite this article in press as: Reinisch et al., Unveiling adipose populations linked to metabolic health in obesity, Cell Metabolism (2024), https://doi.org/10.1016/j.cmet.2024.11.006

tagmentated with Tn5 using the Nextera DNA Flex kit (Illumina, San Diego, CA). All libraries were sequenced on a Novaseq 6000 instrument at Functional Genomics Center Zurich.

Preprocessing and quantification

Only samples with 3 million total reads were used for downstream analyses resulting into 74 visceral AT samples and 68 subcutaneous AT samples with MHO and MUO. The raw reads were first cleaned by removing adapter sequences and poly-x sequences (> 9 nt used for detection) using fastp (version 0.20.0).[42] Reads with length <18nt after trimming were additionally filtered out.

Sequence pseudo alignment of the resulting high-quality reads to the Human reference genome (build GRCh38.p13) and quantification of gene level expression (gene model definition from GENCODE release 32) was carried out using Kallisto v0.46.1.[43] Samples with counts exceeding 20 million were subsequently down-sampled. Down-sampled raw counts were homoscedastically normalized with respect to the library size using the variance stabilizing transformation from the R package DESeq2 v1.44.0.[44] Normalized counts were adjusted for exon mapping rate using the R package limma v3.60.2 for quality control.[45]

For the bariatric surgery cohort, visceral AT samples were processed in the same way as described above.

Differential expression

To detect differentially expressed genes we used the generalized linear model approach implemented in the R package DESeq2 v1.44.0[44] to the raw counts using exon mapping rate as a covariate. Genes showing altered expression with p-value < 0.01 and $|\log_2 FC| > 1$ were considered significant. Differentially expressed genes of the subcutaneous and visceral AT are provided as supplementary table (Table S6).

snRNA-sequencing

Nuclei isolation

Frozen tissues were thawn, carefully minced in lysis Buffer (10 mM Tris-Hcl, 146 mM NaCl, 21 mM MgCl2, 1 mM CaCl2, 0.1 % CHAPs pH=7.4) and grinded by using a tight douncer (Thermo Fisher Scientific, Waltham, MA, United States) on ice. Homogenized tissue was filtered through a 40 μm sieve (Corning, Massachusetts, United States), centrifuged at 500 x g for 5 min at 4 °C to pellet the nuclei and resuspended in buffer supplemented with 1 % BSA and 0.2 U/μL RNAase inhibitor (Takara Bio, Kusatsu, Japan). The nuclei quality, which was defined by a round morphology and no blebbing of nuclei, was inspected by light microscopy.

10X library preparation and sequencing

10X-based libraries were generated following manufacture's protocol (10X Genomics, Pleasanton, CA, United States) for each combination of metabolic health status and sex by pooling the nuclei together (for visceral AT: MHO_W: n= 11, MHO_M: n= 7, MUO_W: n= 15, MUO_M: n= 8, MHNO=6, for subcutaneous AT: MHO_W: n= 17, MHO_M: n= 5, MUO_W: n= 10, MUO_M: n= 4, MHNO= 4). Briefly, 1000 nuclei/μL suspension was loaded to 10X chromium with a 3' V3.1 kit. All libraries were sequenced on a Novaseq6000 instrument (Illumina, Eindhoven, Netherlands) at health 2030 genome center.

snRNA-seq data analysis

The Cell Ranger v.7.1.0 pipeline[46] was used for sample demultiplexing, read alignment against reference genome assembly GRCh38, cell barcode processing and unique molecular identifier (UMI) counting (expected nuclei count was set to 10,000 for visAT samples). The R package Seurat v4.4.0[47,48] was used to process and analyse filtered feature-barcode count matrices. scDblFinder[49] was applied to identify and remove doublets. For quality control, nuclei with unique feature counts < 250 (visAT) / 300 (scAT) or > 4000 (visAT) / 5000 (scAT), UMI counts > 20,000 and mitochondrial gene counts > 5% were discarded from downstream analyses. For each AT depot, samples were normalized via sctransform and integrated using canonical correlation analysis method of Seurat.[47,48] Louvain algorithm was applied to cluster filtered, normalized, and integrated nuclei based on first 30 PCs. Cluster marker genes were identified based on differential gene expression analysis (Wilcoxon rank-sum test with |log2 fold-change| > 0.25 and adjusted p-value < 0.01). Clusters were then annotated into broad cell types based on known markers from literature.[11] For each broad cell type, differential gene expression analysis (Wilcoxon rank-sum test with |log2 fold-change| > 0.25 and adjusted p-value < 0.05) was performed between different conditions using the FindMarkers function from Seurat.[47,48] WikiPathways enrichment of the differentially expressed genes was performed using the R package enrichR v3.2[64] and enriched terms were visualized using the R package SCpubr v2.0.2.[50] Top marker genes, differentially expressed genes for different broad cell types are provided in the supplementary file (Tables S7 and S8).

Adipocytes, MesoCs, APCs and immune cells were selected for each AT depot separately and re-clustered following the same pipeline as mentioned above to identify the different cellular sub types using first 20 PCs. Subcluster marker genes were identified based on differential gene expression analysis (Wilcoxon rank-sum test with |log2 fold-change| > 0.25 and adjusted p-value < 0.01). Subclusters were annotated based on the known markers from literature[10–13] and top marker genes. WikiPathways enrichment of the marker genes was performed for each adipocyte subpopulation using the R package enrichR v3.2[64] and enriched terms were visualized using the R package SCpubr v2.0.2.[50] Marker genes for different cell subpopulations are provided in the supplemental information (Tables S9, S10, S11, and S12).

The cell-cell interaction analysis in the snRNA samples were analyzed using the R package CellChat v1.6.[51] Only visceral APC and immune cell subpopulations were considered for the cell-cell interaction analysis.

snRNA-seq data comparison with published datasets

To compare with the Emont et al. dataset,[11] we used a reference mapping approach to integrate our snRNA-seq datasets separately for each AT depot. We selected only Caucasian individuals from the Emont et al. dataset for this comparison. For each AT depot, we identified anchor cells between our snRNA-seq datasets and the depot-specific reference dataset in a shared low-dimensional space

Please cite this article in press as: Reinisch et al., Unveiling adipose populations linked to metabolic health in obesity, Cell Metabolism (2024), https://doi.org/10.1016/j.cmet.2024.11.006

based on overlapping high-variable features. These anchor cells were then used to project our snRNA-seq datasets onto the reference, transferring cell type labels and metadata to the query dataset. For other published datasets,[10,12–14,33] either individual marker genes were visualized, or enrichment scores were calculated for gene signature in our snRNA-seq datasets using Seurat. Gene enrichment scores were visualized using the R package SCpubr v2.0.2.[50]

Deconvolution of bulk RNA-seq data

Deconvolution of the bulk RNA-sequencing data from both subcutaneous and visceral AT was performed using the R package BisqueRNA v1.0.5,[52] with the corresponding depot-specific snRNA-sequencing data as the reference. Exon mapping rate-adjusted normalized counts were used for the bulk data.

SNP-based demultiplexing

To perform SNP-calling and demultiplexing on the pooled samples, cellsnp-lite (version 1.2.3)[53] was first used to call SNP on a cell-level using the 1000 Genomes-based reference variant call file for hg38 at a resolution of 7.4 million SNPs. SNPs with <20 counts and a <10% minor allele frequency were filtered out, as per the developer recommendations. Finally, the tool vireo (version 0.5.8)[54] was used to demultiplex the pooled data using the cellsnp-lite-derived genotype information.

Pseudobulk analysis

For each broad cell type, raw gene counts were aggregated across nuclei per SNP-demultiplexed individual to generate pseudobulk data. For adipocytes, APCs and MesoCs, pseudobulk count matrices were normalized using the trimmed-mean on M values method in the R package edgeR v4.2.[55] Normalized pseudobulk data was used for principal component analysis.

Multi-cellular factor analysis (MOFA-cell)

Unsupervised multi-cellular factor analysis was to capture sample variability across broad cell types, identifying significant associations with metabolic health status and sex. This analysis was separately conducted for each AT depot on the pseudobulk data of SNP-demultiplexed individuals using the R package MOFAcellulaR v0.0.0.9.[15] Only broad cell types with a minimum of 10 cells per SNP-demultiplexed individual were included in the analysis. Low expressed genes (< 10 counts per individual or detected in < 25% of all individuals) were filtered out from each pseudobulk profile for quality control. Filtered pseudobulk expression profiles were normalized using the trimmed-mean on M values.

For each cell type, the highly variable genes were detected across all samples. Background genes were excluded based on the prior knowledge of cell type specific markers. Filtered highly variable genes per cell types were used as input to train the model using the R package MOFA2 v1.8.[56,57] The trained model represented sample variability across eight and seven well represented cell types in visceral and subcutaneous AT, respectively through six latent factors.

Sample variability was visualized via UMAP representation in a two-dimensional space based on latent factor scores. Statistically significant associations between latent factor scores and metabolic health status or sex were determined using ANOVA. Significantly associated latent factors were further explored and visualized to interpret the model.

Correlation analysis with clinical parameters

Clinical parameter correlation analyses were performed using the *corr.test* function from the R package psych v2.4.3, with multiple testing correction. Non-parametric Kendall and Spearman correlation coefficients were computed for estimated cell type proportions from bulk RNA-seq deconvolution and exon mapping rate-adjusted expressions of genes of interest, respectively.

RNA-scope based stainings

RNAscope Multiplex Fluorescent V2 assay (Bio-techne, Cat. No. 323110) was performed according to the manufacturer's instructions. Briefly, 5 μm thin visceral AT sections were deparaffinized and rehydrated, before antigen retrieval was performed by treating the sections with protease III and boiling them at 98-104°C for 15 minutes in the target-retrieval buffer supplied by the manufacturers. Sections were incubated overnight with the indicated probes (Hs 3plex positive control, 3Plex negative control, Hs-BCHE-C1, Hs-ZNF804B-C1). The channels were revealed with TSA OPAL 570, and TSA Opal 650. Tissues were counterstained with DAPI, mounted with Prolong Gold Antifade Mountant, and were imaged by fluorescence microscopy after signal amplification and secondary antibody incubation.

Statistical analysis

Statistical analyses were performed using GraphPadPrism (version 10) or R v4.4 via RStudio (2023.9.1.494). Statistical significances were determined as described in the figure legends.